**Astronomy
&
Astrophysics**

The multiplicity of exoplanet host stars[*]

Spectroscopic confirmation of the companions GJ 3021 B and HD 27442 B, one new planet host triple-star system, and global statistics

M. Mugrauer[1], R. Neuhäuser[1], and T. Mazeh[2]

[1] Astrophysikalisches Institut, Universität Jena, Schillergäßchen 2-3, 07745 Jena, Germany
  e-mail: markus@astro.uni-jena.de
[2] Tel Aviv University, Tel Aviv 69978, Israel

ABSTRACT

Aims. We present new results from our ongoing multiplicity study of exoplanet host stars and present a list of 29 confirmed planet host multiple-star systems. Furthermore, we discuss the properties of these stellar systems and compare the properties of exoplanets detected in these systems with those of planets orbiting single stars.

Methods. We used direct imaging to search for wide stellar and substellar companions of exoplanet host stars. With infrared and/or optical spectroscopy, we determined the spectral properties of the newly-found co-moving companions.

Results. We obtained infrared H- and K-band spectra of the co-moving companion GJ 3021 B. The infrared spectra and the apparent H-band photometry of the companion is consistent with an M3–M5 dwarf at the distance of the exoplanet host star.

HD 40979 AB is a wide planet host stellar system, with a separation of ∼ 6400 AU. The companion to the exoplanet host star turned out to be a close stellar pair with a projected separation of ∼130 AU, hence, this system is a new member of those rare planet host triple-star systems of which only three other systems are presently known.

HD 27442 AB is a wide binary system listed in the Washington Double Star Catalogue, whose common proper motion was recently confirmed. This system is composed of the subgiant HD 27442 A hosting the exoplanet, and its faint companion HD 27442 B. The visible and infrared J-, H-, and K_S-band photometry of HD 27442 B at the distance of the primary star shows that the companion is probably a white dwarf. Our multi-epochs SofI imaging observations confirm this result and even refine the suggested physical characteristics of HD 27442 B. This companion should be a relatively young, hot white dwarf with an effective temperature of ∼14 400 K, and cooling age of ∼220 Myr. Finally, we could unambiguously confirm the white dwarf nature of HD 27442 B with follow-up optical and infrared spectroscopy. The spectra of the companion show Hydrogen absorption features of the Balmer, Paschen, and Bracket series. With its subgiant primary and the white-dwarf companion, the HD 27442 AB system is the most evolved planet host stellar system known today.

The mass-period and eccentricity-period correlation of planets around single stars and those residing in multiple-star systems seem different for the short-period planets. The distribution functions of planet orbital elements (P, e) are identical, while the mass-distribution ($m \sin(i)$) exhibits one difference. While both planet populations exhibit a peak in their mass-distribution at about 1 M_{Jup}, the frequency of more massive planets continually decreases in single-star systems, whereas the mass-distribution of planets residing in multiple-star systems exhibits a further peak at about 4 M_{Jup}. This indicates that the mass-distributions of the two planet populations might differ in the intermediate mass-range between 2 and 6 M_{Jup}.

Key words. planetary systems

1. Introduction

Planets are believed to form in a gas and dust disk by either gravitational disk instability or accretion. If the planet-bearing disk surrounds a star that is located in a multiple-star system, the stellar companion(s) not only truncate(s) the extent of the disk (see e.g. Pichardo et al. 2005) but also directly alter(s) the planet formation processes. Therefore, the characteristics of planets in multiple-star systems might be different from those of planets orbiting single stars.

For example, Mayer et al. (2005) study the influence of the perturbations of the stellar companion on the gravitational instability scenario of the planet-bearing disk by comparing disks with different properties around single stars to disks in a binary system, with a perturbing stellar companion. The tidal interaction of the stellar disturber induces spiral-like arms in the disks, i.e. regions of increased gas density and temperature.

In particular, intermediate-mass disks (∼50 M_{Jup}) that are gravitationally stable in isolation start to fragment in multiple-star systems, and over-dense gas clumps form along the induced spiral arms, clumps that finally lead to planet formation via disk instability. On the other hand, in more massive disks the induced compressional heating along the dense spiral arms is so strong that the disk remains gravitationally stable, although it would fragment in a single-star system. Hence, stellar multiplicity may either trigger or hamper planet formation via gravitational disk

---

[*] Based on observations obtained on La Silla in ESO programs 70.C-0116(A), 71.C-0140(A), 73.C-0103(A), and on Paranal in ESO runs 074.C-0144(B), 074.C-0144(C), 073.C-0370(A), on Mauna Kea in UKIRT program U/02A/16, as well as at the Munich LMU University Observatory on Mount Wendelstein.

instability, depending on the characteristics of the stellar system, as well as on the disk properties (mass, cooling times).

In the accretion scenario, dust particles accumulate into planetesimals that finally accrete into rocky earth-like planets, while the cores of gas giant planets are formed later on. The accretion process is very sensitive to the relative velocities of the interacting particles. In order that accretion can occur, the relative velocities must not be too high, which would favor destruction of colliding particles. On one hand, a stellar companion induces high particle eccentricities and therefore the relative velocities of colliding objects are substantially increased. On the other hand, there are also dissipative mechanisms (most important here is the gas drag force) that again reduce the induced, high relative velocities. Whether accretion to larger bodies occurs or fragmentation of colliding objects into dust is favored depends on which of these two processes dominates (Marzari & Scholl 2000). Therefore, stellar multiplicity also influences the efficiency of planet formation in the accretion scenario.

Once formed, giant gas planets that remain embedded in the disk continue to accrete material and might also migrate within the disk. According to Kley (2000), stellar companions alter both processes by varying the density structure of the protoplanetary disk. The accretion is enhanced and the migration time reduced, which also damps the orbital eccentricities of the migrating planets.

Finally, after the disappearance of the planet bearing disk, the orbital elements of planets in binary systems can be altered over a long span of time by the Kozai effect, which oscillates the planet eccentricity and can also lead to an orbital migration if the planetary orbital plane is sufficiently inclined to the orbital plane of the stellar system; see. e.g. Ford et al. (2000) and Wu & Murray (2003). Thus, the orbital characteristics of planets residing in multiple-star systems and those orbiting around single stars could show differences that might shed some light on their formation and evolution.

During the decade of extrasolar intensive study, many planets in multiple-star systems were discovered. Already during the first two years of the detection of the first low-mass exoplanet 51 Peg b (Mayor & Queloz 1995), Butler et al. (1997) found three exoplanets residing in double-star systems – 55 Cnc, τ Boo, and υ And. While 55 Cnc and τ Boo were both already known as binary systems, υ And was considered as a single star at that time. Later on, Lowrance et al. (2002) found a co-moving wide companion of υ And, turning it into a planet host binary system. Both υ And and 55 Cnc are wide binaries composed of the bright exoplanet host star and a faint low-mass M-dwarf companion, separated from the planet host star by several hundred AU. The majority of all planet host binaries known today are widely separated pairs like 55 Cnc and υ And. In contrast, τ Boo belongs to the group of those few relatively close planet host binary systems with separations smaller than 100 AU. Only six of those close stellar systems are presently known (see Table 6).

The apparent lack of close binaries hosting planets is probably a selection effect due to the difficulty of detecting planets in close binary systems using the radial-velocity technique (see Sect. 4). If the two components of a binary system cannot be spatially separated by the spectrograph, only the sum of both stellar spectra can be detected (double-lined spectroscopic binary). Even in the case of a high flux ratio between primary and secondary ($F_{Prim}/F_{Sec} \lesssim 100$), the primary spectrum is affected by the parasitic light of the secondary, inducing changes in the line profiles of the primary spectrum. To avoid these perturbations in the planet search, close stellar systems are excluded from the large planet search campaigns studying several thousand F to K stars. Only wide binaries, in which one can take spectra of each component separately, or close systems composed of a bright primary and a much fainter secondary star are targets of these programs.

Nevertheless, planet searches in close binary systems is possible. One can model the spectrum of the system with the sum spectrum of the two components with different radial velocities, as is done by TODCOR (Zucker & Mazeh 1994) or TODMOR (Zucker et al. 2003, 2004). One can use this technique to finally derive the radial velocities of both components, allowing a planet search around both binary components. Today radial-velocity projects are on the way toward searching for planets in wide (Desidera et al. 2004; Toyota et al. 2005) as well as in close (double-lined spectroscopic) binary systems (Konacki 2005b). A first promising result was reported by Konacki (2005a), who found a planet orbiting the primary component of the close triple-star system HD 188753 A/B+C.

Since the detection of the first exoplanets in binaries (Butler et al. 1997), more and more exoplanet host stars, once considered as single stars, turned out to be components of multiple-star systems, detected in imaging programs that search for visual companions of exoplanet host stars. In order to find both close and wide companions, these imaging campaigns are carried out with high-contrast, small-field adaptive optics and with normal seeing-limited imaging (large field of view). Patience et al. (2002) detected a close companion to HD 114762. Furthermore, Els et al. (2001) report on a faint companion only 2 arcsec separated from Gl 86, that eventually turned out to be a white dwarf (Jahreiß 2001; Mugrauer & Neuhäuser 2005; Lagrange et al. 2006). Finally, Mugrauer et al. (2004a,b, 2005, 2006) present 7 new wide companions of exoplanet host stars, namely HD 89744, HD 75289, HD 16141, HD 114729, HD 196050, HD 213240, and HD 46375.

In this paper we publish additional results of our multiplicity study. We present our imaging and photometric data for the companions GJ 3021 B, HD 27442 B (see also Chauvin et al. 2006; Raghavan et al. 2006) and report a new co-moving companion to the planet host star HD 40979 in Sect. 2. In Sect. 3 we summarize the results of the infrared and optical follow-up spectroscopy of GJ 3021 B and HD 27442 B. In Sect. 4 we compile an updated list of confirmed planet host multiple-star systems and discuss their properties. Finally, in Sect. 5, we compare the masses and orbital parameters of planets residing in multiple-star systems with those of planets orbiting single stars.

2. Astrometry and photometry

GJ 3021 and HD 27442 are targets of our southern search program for the visual companions of exoplanet host stars. Observations were carried out with the infrared camera SofI[1], a 1024×1024 HgCdTe-detector installed at the Nasmyth focus of the 3.58 m NTT[2] telescope. To be sensitive to faint substellar companions, all targets were observed in the near infrared H-band at $1.6 \mu m$, where companions with masses as low as a few tens of Jupiter masses come into the range of a 4 m class telescope. Most of the exoplanet host stars are located within a distance of about 60 pc around the sun, thus all are relatively bright sources in the night sky. In order to avoid strong saturation effects, we used the smallest available pixel scale and shortest available detector integration times. We observed all targets in the SofI small-field mode with its

---

[1] Son of ISAAC.

[2] New Technology Telescope.

Table 1. The astrometrical calibration of SofI, UFTI (IR), and MONICA (Optical) in the individual observing runs.

instrument	epoch	PS [arcsec/pixel]	PA [°]
SofI$_{small}$	12/02	0.14366 ± 0.00016	90.069 ± 0.041
SofI$_{small}$	06/03	0.14365 ± 0.00013	90.069 ± 0.032
SofI$_{small}$	07/04	0.14356 ± 0.00011	90.047 ± 0.024
UFTI	11/02	0.09098 ± 0.00043	0.770 ± 0.087
UFTI	10/03	0.09104 ± 0.00030	0.711 ± 0.083
MONICA	11/04	0.49051 ± 0.00015	0.003 ± 0.035
MONICA	07/05	0.49042 ± 0.00029	−0.013 ± 0.063

Fig. 1. The SofI small-field image of the planet host star GJ 3021 (central bright star A with diffraction spikes and reflections), taken in December 2002 in the H-band, with a total integration time of 10 min. Only two companion candidates are detected with $S/N \geq 10$ close to the exoplanet host star. GJ 3021 B is co-moving to the exoplanet host star. The star R, whose proper motion is listed in the UCAC2 catalogue is used as the astrometric reference.
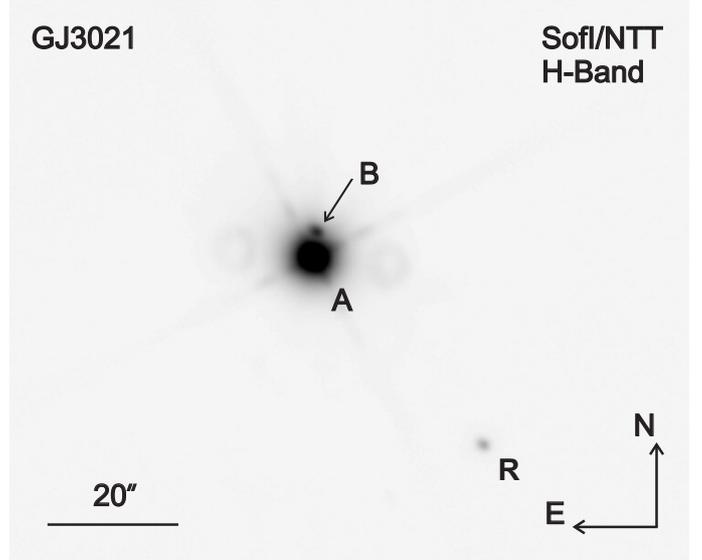
pixel scale of 144 mas per pixel, yielding a field of view of 147 arcsec × 147 arcsec. The spacial resolution samples the typical seeing conditions well, which are better than 1 arcsec at the La Silla ESO Observatory. Therefore, the proper motions of detected objects can be determined after one year with a precision of 20 to 30 mas over the whole SofI field of view. Besides the detection of wide companions, the small pixel scale also allows the detection of close companions (see e.g. GJ 3021 B), which are separated from the bright star by only a few arcsec. Only very close companions with a separation of less than about 2 arcsec remain hidden in the glare of the primary star. Those can be revealed only by high-contrast AO imaging (see e.g. Mugrauer & Neuhäuser 2005).

We took 10 images per target, each of which is an average of 50 × 1.2 s integrations, i.e. 10 min of total integration time per target. In order to cancel out the high infrared background we applied the standard jitter technique; i.e. the telescope is moved by a few arcsec to a new position before the next image is taken. Hence, each object is located at a different position on the detector at the different images, a fact that allows the determination of the infrared background at each pixel. The background estimation and subtraction, as well as the flat-fielding of all images, is achieved with the ESO package *ECLIPSE*[3] (Devillard 2001), which finally also combines all images, using a shift+add procedure.

The astrometry of all SofI images is calibrated with the 2MASS[4] point source catalogue (Cutri et al. 2003), which contains accurate positions of objects brighter than 15.2 mag in H ($S/N > 5$). The derived pixel scale PS and detector orientation PA of all observing runs, whose data are presented in this paper, are summarized in Table 1. The SofI detector is tilted by PA from north to west.

2.1. GJ 3021

GJ 3021 (HD 1237) is a nearby G6V dwarf (Perryman & ESA 1997, ~18 pc Hipparcos), located in the southern constellation Hydrus. Naef et al. (2001b) detected a massive exoplanet ($m \sin(i) = 3.37\,M_{Jup}$) with a period of 134 days and an eccentric ($e = 0.511$) orbit with a semi-major axis of 0.49 AU. According to Naef et al. (2001b), the star is a photometric variable and exhibits a high level of chromospherical activity. Its spacial velocity ($U = 33.7\,\mathrm{km\,s^{-1}}$, $V = 17.4\,\mathrm{km\,s^{-1}}$, $W = 2.8\,\mathrm{km\,s^{-1}}$) metallicity [Fe/H] = 0.1 ± 0.08, chromospheric activity level $\log(R'_{HK}) = -4.27$, as well as its lithium abundance $\log(N(\mathrm{Li})) = 2.11 \pm 0.08$, are all typical of members of the Hyades super cluster. The chromospherical age ranges from 0.02 to 0.8 Gyr, which is consistent with an age of 0.5 Gyr, as derived by

Rocha-Pinto & Maciel (1998) and with the age estimate of 0.15 to 0.25 Gyr from Saffe et al. (2005).

We obtained a first image of GJ 3021, shown in Fig. 1, in December 2002. Follow-up, second-epoch observations were carried out in June 2003. Only two companion candidates were detected with $S/N \geq 10$ in the SofI images. The closer one (B) is located only ~4 arcsec north of GJ 3021, and the other candidate (R) is detected ~39 arcsec southwest of the exoplanet host star. Both objects could be either real companions of the exoplanet host star or just background stars randomly located close to but far behind the exoplanet host star. Because of its proximity to the sun, GJ 3021 exhibits a high proper motion ($\mu_\alpha \cos(\delta) = 433.88 \pm 0.55$ mas/yr, $\mu_\delta = -57.91 \pm 0.45$ mas/yr), derived from precise measurements of the European astrometry satellite Hipparcos (Perryman & ESA 1997), which also provided the parallax of the star ($\pi = 56.76 \pm 0.53$ mas). Real companions of the exoplanet host star must share the proper motion of their primary stars, as their orbital motion is much smaller than the proper motion. Such co-moving companions can therefore be distinguished from non-moving or slowly moving background stars by comparing two images taken with a sufficiently long time difference.

The more distant star, R, is listed in the UCAC2 catalogue (Zacharias et al. 2004) with a proper motion $\mu_\alpha \cos(\delta) = 1.8 \pm 5.9$ mas/yr and $\mu_\delta = -24.9 \pm 6.1$ mas/yr, which is significantly different from the proper motion of the exoplanet host star. Hence, we can clearly rule out the companionship of this candidate, which is only a slow-moving object, most probably located in the background.

Recently, Chauvin et al. (2006) have also shown that the closer companion candidate (HD 1237 B) shares the proper motion of the planet host star. By comparing the two SofI images, we can confirm this astrometric detection. The measured proper motion of the companion between the two SofI observing epochs is $PM_{Ra} = 368 \pm 68$ mas, $PM_{Dec} = -48 \pm 68$ mas, which is consistent with the expected proper motion of the exoplanet host

---

[3] ESO C Library for an Image Processing Software Environment.
[4] 2 Micron All Sky Survey.

Table 2. The separations and position angles of GJ 3021 B and HD 27442 B relative to their primaries for all SofI observing epochs.

GJ 3021 B	epoch	sep[arcsec]	PA[°]
	NTT 12/02	3.892 ± 0.076	355.480 ± 0.858
	NTT 06/03	3.810 ± 0.075	354.570 ± 0.902
HD 27442 B	epoch	sep[arcsec]	PA[°]
	NTT 12/02	12.933 ± 0.083	36.400 ± 0.364
	NTT 07/04	12.940 ± 0.079	36.980 ± 0.347
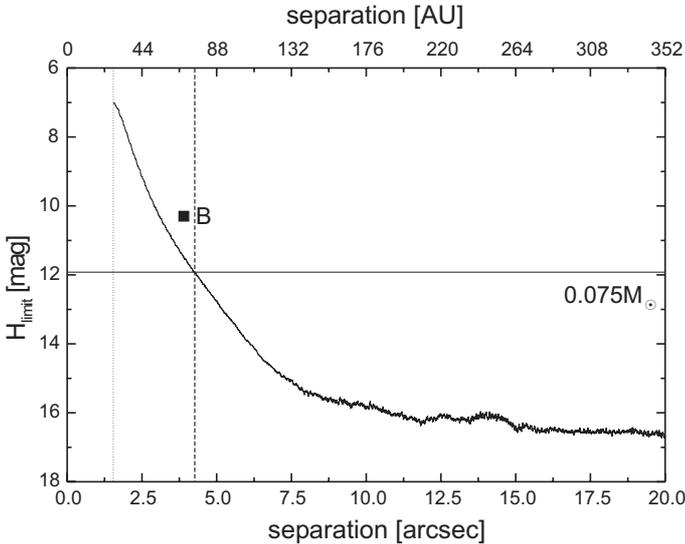
Fig. 2. The detection limit ($S/N = 10$) of the SofI H-band imaging of GJ 3021 for a range of separations given in arcsec at the bottom and as projected separation in AU at the top. Saturation occurs at ~1.5 arcsec (dotted line), i.e. companions with a projected separation closer than 26 AU are not detectable. At a system age of 0.5 Gyr, all stellar companions ($m \geq 75 M_{\rm Jup}$) are detectable beyond the distance illustrated by the dashed line (~74 AU).

star ($PM_{\rm Ra} = 317 \pm 1$ mas, $PM_{\rm Dec} = -6 \pm 1$ mas) for the given timespan. The separation and position angle of GJ 3021 B relative to its primary at both SofI observing epochs are summarized in Table 2.

By measuring the noise level in the individual SofI images of both observing runs, we derived the detection limits of the SofI observations. Figure 2 shows the achieved detection limit ($S/N = 10$) for a range of separations to the planet host star for a system age of 0.5 Gyr. Due to the low declination of GJ 3021, our SofI observations were always carried out at high airmasses ($AM \geq 1.5$) with an average $FWHM$ of only ~1.5 arcsec. A limiting magnitude of 16.7 mag is reached in the background-limited region, i.e. at angular separations around GJ 3021 A larger than 15 arcsec. If we assume a system age of 0.5 Gyr, the achieved limiting magnitude enables the detection of brown-dwarf companions with a mass $m \geq 19 M_{\rm Jup}$, derived with the Baraffe et al. (2003) models and their magnitude-mass relation. This mass-limit increases for higher system ages, e.g. 56 $M_{\rm Jup}$ at 5 Gyr.

Objects with angular separations of up to 63 arcsec (~1100 AU) around the exoplanet host star are imaged twice in both SofI observing runs. The SofI field of view is about 4.5 times larger than the field of view investigated by Chauvin et al. (2006) using NACO and its S27 camera. Wide companion candidates, which lie outside the small AO field of view (see e.g. object R), can be detected only with SofI. In contrast, faint close companions that need higher contrast can only be found with adaptive optics, like NACO. Hence, both the seeing-limited and

the diffraction-limited observations yield complementary information about the multiplicity of the planet host star for different ranges of angular separation. In the case of GJ 3021 A, our SofI images can rule out any other wide co-moving companion, expect GJ 3021 B. Combining our SofI imaging data with the NACO observations obtained by Chauvin et al. (2006), additional stellar companions ($m \geq 75 M_{\rm Jup}$) can be ruled out around GJ 3021 A with projected separations from ~20 AU up to ~1110 AU.

We measured the companion photometry in both SofI images and obtained an apparent H-band magnitude $H = 10.298 \pm 0.054$ mag, consistent with the NACO photometry presented by Chauvin et al. (2006). With the given distance of the exoplanet host star, we obtained an absolute H-band magnitude of the companion $M_H = 9.068 \pm 0.058$ mag. According to the magnitude-mass relation of the Baraffe et al. (1998) evolutionary models and the color-spectral type conversion from Kenyon & Hartmann (1995), the companion photometry is consistent with an M4-M5 dwarf with a mass of $0.125 \pm 0.003 M_\odot$ at an age of 0.5 Gyr. This estimate, derived only by photometry, still has to be confirmed by spectroscopy (see Sect. 3).
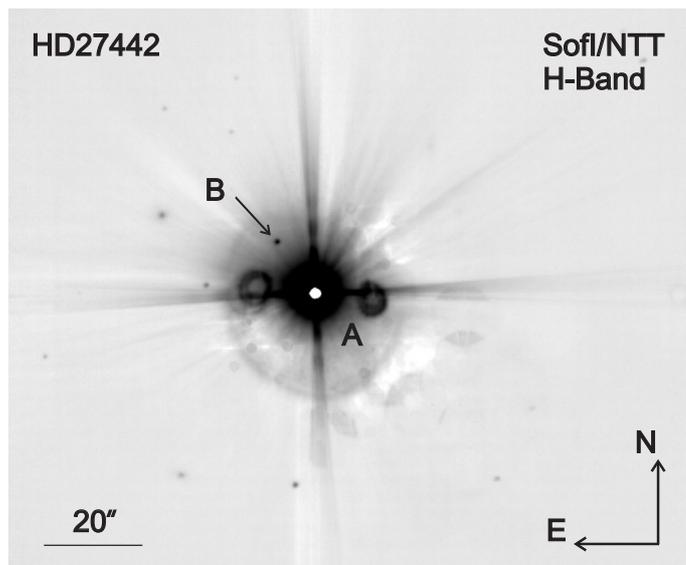
2.2. HD 27442

HD 27442 (ϵ Ret) is ~10 Gyr old K2 subgiant (Randich et al. 1999) located at a distance of ~18 pc ($\pi = 54.84 \pm 0.50$ mas) from the sun, derived by Hipparcos (Perryman & ESA 1997). According to Santos et al. (2004) HD 27442 exhibits a surface gravity of $\log(g) = 3.55 \pm 0.32$ cm s^{-2}. The age estimate of the star, as well as its surface gravity, is fully consistent with the subgiant classification. Butler et al. (2001) detected an exoplanet ($m \sin(i) = 1.35 M_{\rm Jup}$) in an almost circular orbit ($e = 0.058$) around HD 27442 with an orbital period of 415 days and a semi-major axis of 1.16 AU.
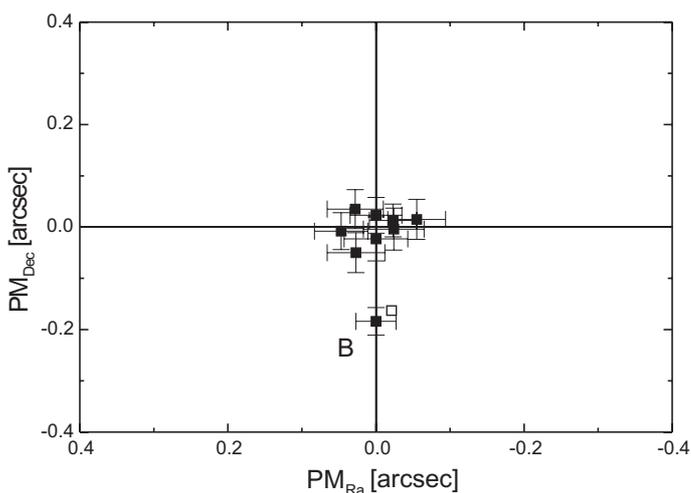
HD 27442 is listed in the WDS[5] catalogue (Worley & Douglass 1997) as a binary system with a $V = 12.5$ mag companion, based on two astrometric measures in 1930 and one follow-up observation in 1964. In 1930 the companion was located at a separation of 13.7 ± 0.1 arcsec and at a position angle of $35 \pm 1°$. Recently, Chauvin et al. (2006) and Raghavan et al. (2006) also reported on their observations of the HD 27442 system. Both groups could clearly detected the companion HD 27442 B close to its primary HD 27442 A and confirmed that HD 27442 A and B form a common proper-motion pair. We observed HD 27442 with SofI in December 2002 and July 2004. Our first-epoch H-band image is shown in Fig. 3. After 10 min of total integration, several faint companion candidates were detected close to the bright exoplanet host star. The co-moving companion HD 27442 B is shown in Fig. 3, and the SofI astrometry of HD 27442 B relative to the planet host star is summarized in Table 2.

In our SofI H-band images, several wide companion candidates were detected that are separated from the bright planet host star by up to 64 arcsec (~1200 AU). By comparing the first-epoch with the second-epoch SofI image, the proper motions of all these companion candidates can be determined for the given epoch difference and are shown in Fig. 4. HD 27442 B clearly shares the proper motion of HD 27442 A, confirming the astrometric measurements of Chauvin et al. (2006) and Raghavan et al. (2006). Expect for HD 27442 B, no additional co-moving companions could be identified around the exoplanet host star within the SofI field of view.
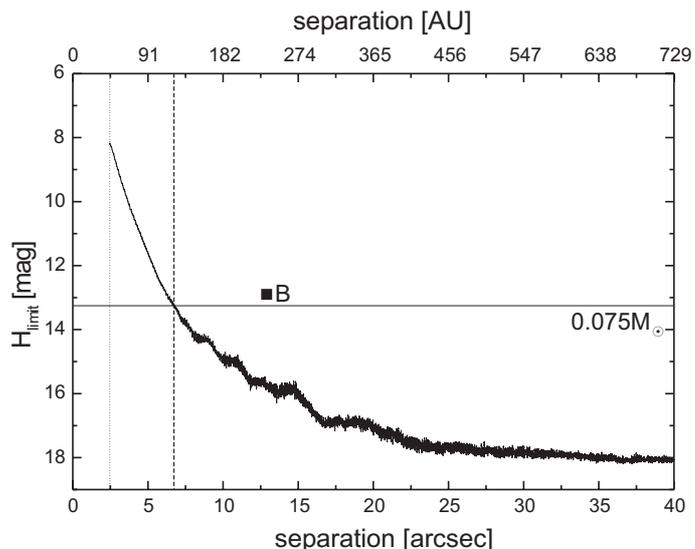
---

[5] Washington Double Star.

Fig. 3. The first-epoch SofI small-field image of the exoplanet host star HD 27442 observed in December 2002. The total integration time of this *H*-band image is 10 min. Several faint companion candidates were detected (*S/N* > 10). The co-moving companion HD 27442 B is visible about 13 arcsec northeast of the bright exoplanet host star.

Fig. 5. The detection limit (*S/N* = 10) of our SofI *H*-band images of HD 27442 for a range of angular separations given in arcsec at the bottom and as projected separations in AU at the top. At ~2.5 arcsec saturation occurs (doted line), i.e. companions with a projected separation closer than 46 AU are not detectable. At a system age of 10 Gyr all stellar companions ($m \geq 0.075\,M_\odot$) are detectable beyond 6.8 arcsec (~125 AU), as illustrated by a dashed line.

Fig. 4. The derived proper motion of all companion candidates detected in our NTT images (*S/N* > 10) from epochs 12/02 and 07/04. The expected proper motion of the primary is derived from Hipparcos data and is shown as a small white square in the plot.

The SofI detection limit versus distance to HD 27442 A is illustrated in Fig. 5. In both SofI images, the seeing is ~0.8 arcsec and a limiting magnitude (*S/N* = 10) of *H* = 18.0 mag is reached beyond ~30 arcsec (547 AU) in the background-limited region. According to Baraffe et al. (2003), the limiting magnitude allows the detection of substellar companions with masses down to 0.055 $M_\odot$ at the approximated age of the exoplanet host star of 10 Gyr. With the high-contrast AO observations obtained by Chauvin et al. (2006) and our SofI wide-field imaging data of the HD 27442 AB system, additional stellar companions of the exoplanet host star, with projected separations between ~30 AU and 1200 AU, can be ruled out.

Chauvin et al. (2006) combined their *J*- and K_S-band NACO photometry of HD 27442 B with its visible magnitude listed in the WDS catalogue and concluded that the companion photometry is inconsistent with a main sequence star or a brown dwarf

at the distance of the exoplanet host star. Instead, the photometry of the co-moving companion is consistent with what is predicted by the evolutionary model of Bergeron et al. (2001) for white dwarfs with hydrogen- or helium-rich atmospheres, with a mass ranging between 0.3 and 1.2 $M_\odot$ and an effective temperature ranging between 9000 and 17 000 K.

We can confirm the white dwarf hypothesis by comparing the visible WDS and SofI *H*-band photometry of HD 27442 B with known white dwarfs. The average *H*-band photometry of HD 27442 B in the two SofI images is *H* = 12.871 ± 0.085 mag, which is consistent with a M_H = 11.566 ± 0.087 mag object at the distance of the exoplanet host star. With *V* = 12.5 ± 0.1 mag from the WDS catalogue, this yields the color of the companion *V* − *H* = −0.37 ± 0.13 mag. Figure 6 shows HD 27442 B in a color-magnitude (M_H − *V* − *H*) diagram, together with the known white dwarfs from the Palomar Green Survey (Liebert et al. 2005), and old white dwarfs from Bergeron et al. (2001). Most of the white dwarfs are well-separated from the isochrone of low-mass stellar objects. They are faint and much bluer than low-mass stellar objects with a similar brightness. Only the youngest (age ≤ 0.29 Gyr), hottest (*T* ≤ 70 000 K), and therefore almost brightest white dwarfs in the comparison sample extend to the upper-right corner of the diagram reaching the stellar isochrone. These relatively young white dwarfs are brighter and redder than their older analogues.

The photometry of HD 27442 B is consistent with a white dwarf companion at the distance of the exoplanet host star. We find several white dwarfs in the Palomar Green Survey with *V*- and *H*-band magnitudes that are comparable with those of HD 27442 B. The properties of these white dwarfs are summarized in Table 3.

Finally, the white dwarf nature of HD 27442 B, derived so far only from colors and absolute magnitudes, has to be confirmed with spectroscopy. Therefore, we obtained follow-up spectra of the companion, which are presented in Sect. 3.
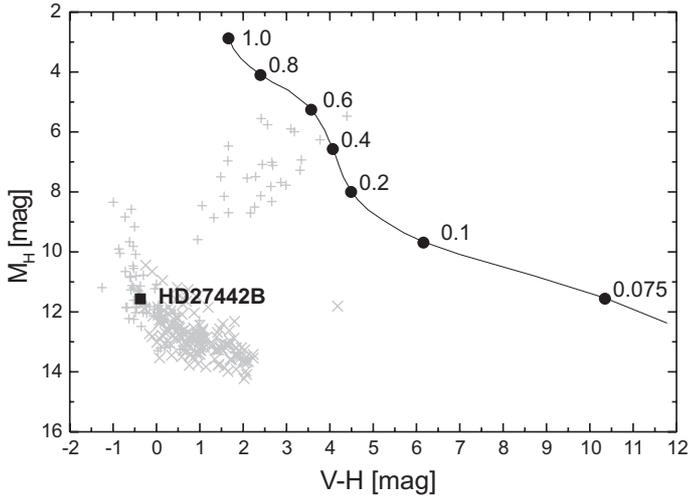
Fig. 6. The $M_H - (V - H)$ color–magnitude diagram for main-sequence stars, white dwarfs, and HD 27422 B. The 8 Gyr isochrone from the Baraffe et al. (1998) models is shown as a solid line, plotted for stellar masses from 0.072 to 1 $M_\odot$. The masses of objects on the isochrone are indicated with black circles. For comparison we show the location of white dwarfs from Bergeron et al. (2001) (X symbols) and from Liebert et al. (2005) (+ symbols).

Table 3. Properties of comparison white dwarfs from the Palomar Green Survey whose absolute V- and H-band photometry is comparable to HD 27442 B.

$T_{\rm eff}$	$14\,400 \pm 3100$ K
$\log(L[L_\odot])$	-2.09 ± 0.22
$\log(g[\mathrm{cm\,s^{-2}}])$	7.95 ± 0.17
$\log(\tau[\mathrm{yr}])$	8.35 ± 0.14
mass	$0.58 \pm 0.11\ M_\odot$

2.3. HD 40979

HD 40979 is located in the northern constellation Auriga. This star is a nearby F8 dwarf at a distance of 33 pc, as derived by Hipparcos (Perryman & ESA 1997). According to Fischer et al. (2003) this star shows a strong lithium absorption feature $\log N(\mathrm{Li}) = 2.79$ but exhibits only a moderate chromospheric activity $\log R'_{HK} = -4.63$. They conclude that the lithium abundance of HD 40979, its color $B - V = 0.537 \pm 0.007$ mag (data from Hipparcos see Perryman & ESA 1997), as well as its Ca H and K emission, are all consistent with a 1.1 to 1.2 $M_\odot$ dwarf at an age of about 1.5 Gyr. Furthermore, they report a periodical modulation of the stellar radial velocity with a period of 263 days. They suggest that this variation is induced by an exoplanet ($m \sin(i) = 3.28\ M_{\rm Jup}$) that orbits the star on an eccentric ($e = 0.25$) orbit with a semi-major axis of 0.83 AU.

HD 40979 is a target of our imaging search campaign for visual companions of northern exoplanet host stars, which is being carried out with the 3.8 m United Kingdom Infrared Telescope (UKIRT), located at Mauna Kea (Hawaii). We took H-band images of all northern targets with the infrared camera UFTI[6], which is equipped with a 1024×1024 HgCdTe infrared detector, providing a pixel scale of ~91 mas per pixel and a 93 arcsec × 93 arcsec field of view. In order to reduce saturation effects we always used the shortest possible detector integration time (4 s) and add up 6 integrations per jitter position. We always chose 24 jitter positions, yielding a total integration time

---

[6] UKIRT Fast Track Imager.
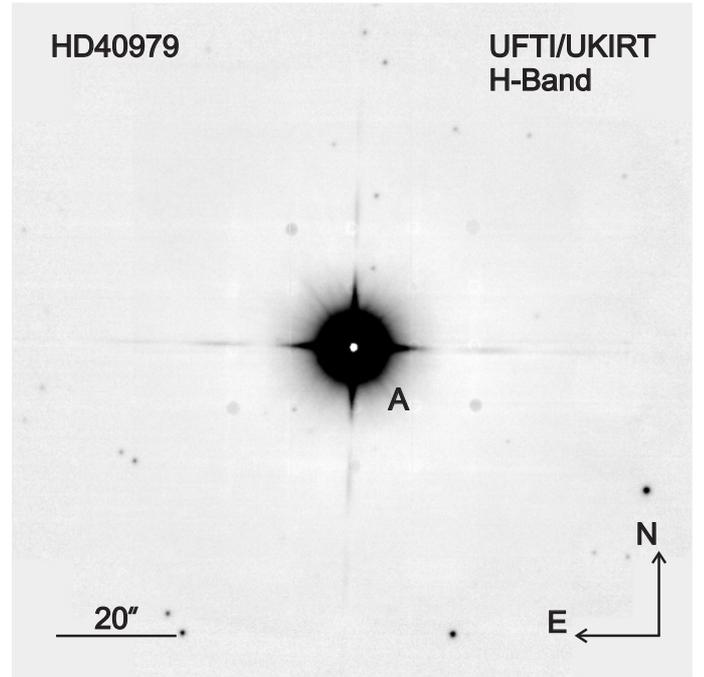
Fig. 7. Our first-epoch UFTI image of the exoplanet host star HD 40979, observed in November 2002 in the H-band. Within the UFTI field of view, several faint companion candidates ($S/N > 10$) were detected around the exoplanet host star. The proper motion of those candidates are shown in Fig. 8.

of 9.6 min per target. The data reduction was carried out again with ESO *ECLIPSE* (Devillard 2001).

We observed HD 40979 the first time in November 2002 with a second-epoch observation one year later in October 2003. The first-epoch H-band image is shown in Fig. 7. By comparing both UFTI images, we obtain the proper motions of all companions-candidates ($S/N > 10$), which are detected in both UFTI images. The expected proper and parallactic motion of the exoplanet host star between our first and second-epoch imaging is well-known from precise Hipparcos astrometry ($\mu_\alpha \cos(\delta) = 95.05 \pm 0.87$ mas/yr, $\mu_\delta = -152.23 \pm 0.47$ mas/yr and $\pi = 30.00 \pm 0.82$ mas). The measured proper motions of all detected companion candidates in our UFTI images are shown in Fig. 8. All detected objects around HD 40979 emerge as slowly moving stars that are unrelated to the exoplanet host star, most probably located far away in the background.
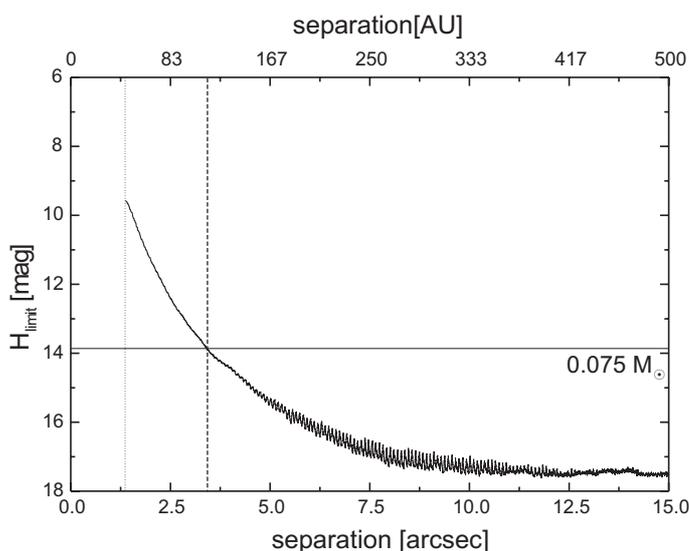
The detection limit of our UFTI observations is shown in Fig. 9. Objects within a radius of ~53 arcsec (~1800 AU) around the exoplanet host star are detected in both UFTI images. In the background-limited region at separations larger than ~10 arcsec (350 AU), a limiting magnitude of $H = 17.5$ mag is reached. According to the Baraffe et al. (2003) models at an assumed system age of 1 Gyr, this limiting magnitude enables the detection of substellar companions with masses, down to 0.032 $M_\odot$. All stellar companions ($m > 0.075\ M_\odot$) are detectable beyond 3.4 arcsec (~110 AU).

Although we did not discover any companion to HD 40979, Halbwachs (1986) reported that this star has a known co-moving companion, with a wide angular separation of 192.5 arcsec (~6400 AU). The proper motion of the co-moving companion HD 40979 B is listed in the UCAC2 catalogue ($\mu_\alpha \cos(\delta) = 93.8 \pm 0.7$ mas/yr, $\mu_\delta = -154.0 \pm 0.7$ mas/yr). Due to the large angular separation between the two stars, the co-moving companion lies outside the UFTI field of view, but is
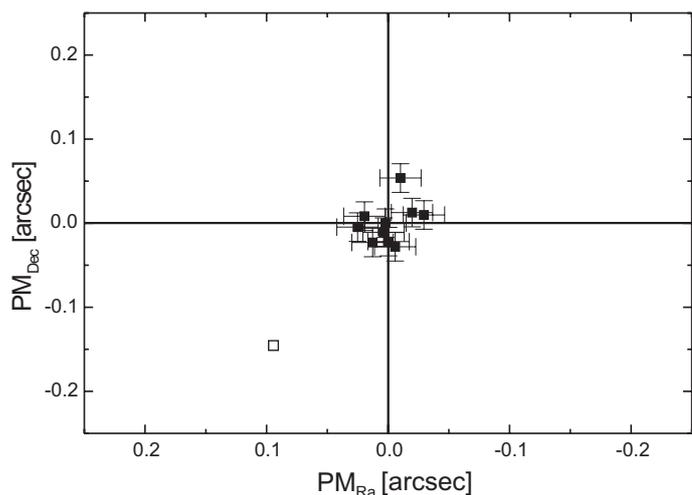
Fig. 8. The measured proper motions of all detected companion candidates within the UFTI field of view around the exoplanet host star HD 40979. The expected proper motion of a co-moving companion is shown by a white small box that is derived with the given epoch difference and the Hipparcos astrometry of the exoplanet host star. All detected objects turn out to be slow-moving background stars.

Fig. 9. The detection limit of our UFTI images of HD 40979 for a range of separations given in arcsec at the bottom and as projected separation in AU at the top. At ~1.4 arcsec (47 AU), saturation occurs (dotted line). At an assumed system age of 1 Gyr all stellar companions ($m \geq 0.075\,M_{\odot}$) are detectable beyond 3.4 arcsec (~110 AU), see dashed line.

detected in the 2MASS image, together with the exoplanet host star. The upper panel of Fig. 10 shows the J, H, and K_S 2MASS images of the co-moving companion HD 40979 B. Note that the companion appears elongated in the northeast direction, which is different from the diffraction patterns of the nearby stars. The elongated diffraction pattern might indicate that there is an unresolved faint object located only a few arcsec northeast of the wide co-moving companion HD 40979 B.

In order to confirm this result, we observed HD 40979 B with the 0.8 m telescope of the Munich LMU University Observatory, located on Mount Wendelstein (Bavaria, south Germany). This telescope is equipped with the CCD-camera MONICA (MOnochromatic Image CAmera), a 1024×1024 SiTe CCD-array (Textronik TK 1024) with a pixel scale of ~490 mas per
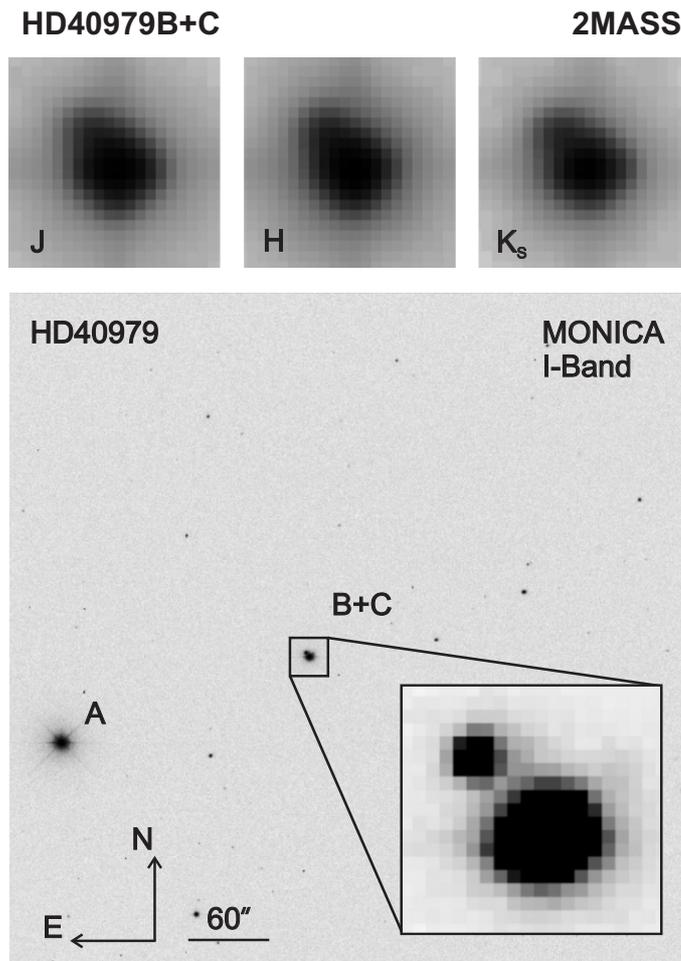

Fig. 10. The 2MASS J-, H-, and K_S-band images (*top panel*) of HD 40979 B and one of our first-epoch MONICA images (*bottom panel*), which shows all components of the triple-star system HD 40979. The pattern of HD 40979 B in the three 2MASS images appears elongated, which is a first hint that there might be an additional faint object located only a few arcsec northeast of HD 40979 B. This object is clearly separated from HD 40979 B in our MONICA images.

pixel and a large field of view of $8.4\,\mathrm{arcmin} \times 8.4\,\mathrm{arcmin}$. We observed the common-proper-motion pair for the first time in November 2004 in the I-band (see Fig. 10). Due to the large MONICA field of view both binary components HD 40979 A and B are detected on the CCD. In order to avoid saturation, we used an exposure time of only 1 s. In total nine I-band images were taken and one of these images is shown in the lower pattern of Fig. 10.

As already indicated by the elongated diffraction pattern of HD 40979 B in the 2MASS images, there is indeed a faint object that is located northeast of HD 40979 B. Because of their small angular separation (~3.9 arcsec), the two stars are not resolved in 2MASS images, whose pixel scale is 1 arcsec per pixel, but clearly stand out in our MONICA I-band images. The faint object might be either an additional companion of the system or just an ordinary background star. To find out if the faint star is really associated with HD 40979 B, we carried out in July 2005 follow-up second-epoch observations with the same image preset.

In a first step, we compared our second-epoch MONICA images with the 2MASS images and determined the proper motions of all objects that appear in the two sets of images (see
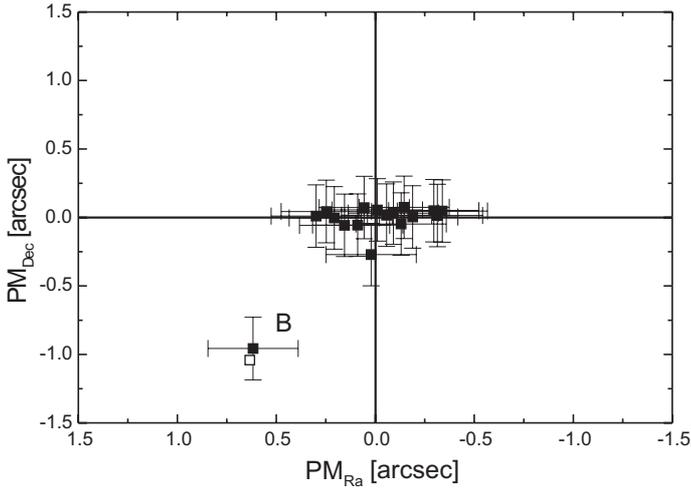
Fig. 11. The derived proper motions of all objects detected around the exoplanet host star HD 40979 A. Comparison is between our second epoch MONICA images taken in July 2005 and the 2MASS images from 1998. The expected proper motion of a companion who shares the proper motion of the exoplanet host star object is indicated as a small white square in the plot.

Table 4. The separations and position angles of HD 40979 B relative to the exoplanet host star HD 40979 A.

HD 40979 B	epoch	sep[arcsec]	sep $_{if\ bg}$ [arcsec]
	2MASS 11/98	192.489 ± 0.085	—
	Wend 11/04	192.586 ± 0.070	193.329
	Wend 07/05	192.351 ± 0.114	193.432
HD 40979 B	epoch	PA [°]	PA $_{if\ bg}$ [°]
	2MASS 11/98	289.230 ± 0.030	—
	Wend 11/04	289.275 ± 0.037	289.432
	Wend 07/05	289.256 ± 0.063	289.459

Fig. 11). HD 40979 B and the exoplanet host star HD 40979 A clearly form a common-proper-motion pair, whereas all other detected objects emerge as unrelated slow-moving objects. The separations and position angles of HD 40979 B relative to its primary star for all three observing epochs are listed in Table 4. They are constant within the astrometric uncertainties as expected for a common-proper-motion pair. We also list the expected variation in separation and position angle if HD 40979 B is a non-moving background source, using the proper and parallactic motion of the exoplanet host star (see the columns sep $_{if\ bg}$ and PA $_{if\ bg}$).

The newly detected faint companion candidate, located northeast of HD 40979 B is well-resolved in both MONICA images. We measured its separation and position angle relative to HD 40979 B in both MONICA images and summarize all results in Table 5. If the companion candidate is a non-moving background object, we expect a change in the separation and position angle due to the proper and parallactic motion of HD 40979 B between the observations. The expected variation in both parameters is given in Table 5. The position angle has to change significantly in the case of a non-moving background source (see sep $_{if\ bg}$ and PA $_{if\ bg}$) but the position angle and separation of the faint object remain constant within their uncertainties in both MONICA images. Hence, this faint object is a co-moving companion of HD 40979 B and is therefore denoted as HD 40979 C. We therefore conclude that the wide binary HD 40979 is a triple-star system, with the exoplanet host star HD 40979 A as primary

Table 5. The separations and position angles of HD 40979 C relative to HD 40979 B.

HD 40979 C	epoch	sep[arcsec]	sep $_{if\ bg}$ [arcsec]
	Wen 11/04	3.857 ± 0.014	—
	Wen 07/05	3.877 ± 0.013	3.913
HD 40979 C	epoch	PA [°]	PA $_{if\ bg}$ [°]
	Wen 11/04	37.811 ± 0.215	—
	Wen 07/05	37.969 ± 0.178	35.972

and a widely separated secondary pair whose components are separated by 129 AU (projected separation).

We measured the apparent I-band magnitudes of HD 40979 B and C in our first and second-epoch MONICA images and obtained I(B) = 7.98 ± 0.03 mag and I(C) = 11.3 ± 0.1 mag. With the distance of the exoplanet host star, we find that the absolute I-band magnitudes of both companions are M_I(B) = 5.37 ± 0.07 mag and M_I(C) = 8.67 ± 0.12 mag. Converting their I-band magnitudes to masses with the Baraffe et al. (1998) models, we obtain, for a system age of 1 Gyr, a mass of 0.833 ± 0.011 $M_\odot$ for HD 40979 B and 0.380 ± 0.025 $M_\odot$ for HD 40979 C, respectively. These mass-estimates do not change significantly for system ages between 1 and 10 Gyr.

3. Spectroscopy

In this section we present our spectroscopic observations of the two co-moving companions GJ 3021 B and HD 27442 B, which confirm their companionship to the exoplanet host stars.

3.1. Near infrared spectroscopy of GJ 3021 B and HD 27442 B

We obtained near infrared H- and K-band spectra of GJ 3021 B and HD 27442 B in October and December 2004 at Paranal Observatory. We used the Infrared Spectrometer And Array Camera (ISAAC), which is mounted at one of the Nasmyth foci of UT1 (Antu). ISAAC is equipped with a 1024×1024 Hawaii Rockwell IR detector (~0.148 arcsec per pixel) for imaging and spectroscopy in the near infrared J-, H-, and K-bands. We used the low-resolution grism, together with the order sorting filters SH (H-band) and SK (K-band), as well as the 1 arcsec slit that yields a resolving power $\lambda/\Delta\lambda$ of ~500 in H and ~450 in the K-band with dispersions of 4.8 Å per pixel and 7.2 Å per pixel, respectively.

Background subtraction was obtained by a 45 arcsec nodding between two positions along the slit. In addition we applied a 5 arcsec random jitter around the two nodding positions to avoid the individual pixels always seeing the same part of the sky. We obtained 16 spectra per target each with an integration time of 60 s. All spectra were flat-fielded using internal lampflats and wavelength-calibrated with Xenon and Argon arclamps. After background subtraction, flat-fielding and wavelength calibration, all done with standard *IRAF* routines, the individual spectra were finally averaged.

The reduced spectra of GJ 3021 B and HD 27442 B were calibrated with the telluric standard stars HD 50491 (B4V) and HD 48215 (B5V), respectively. The spectra were always taken directly after the science spectra with a maximal airmass difference of only ~0.2 dex. We determined the response function of the spectrograph with the spectra of the spectroscopic standard stars and reference spectra from Pickles (1998). The *H*- and
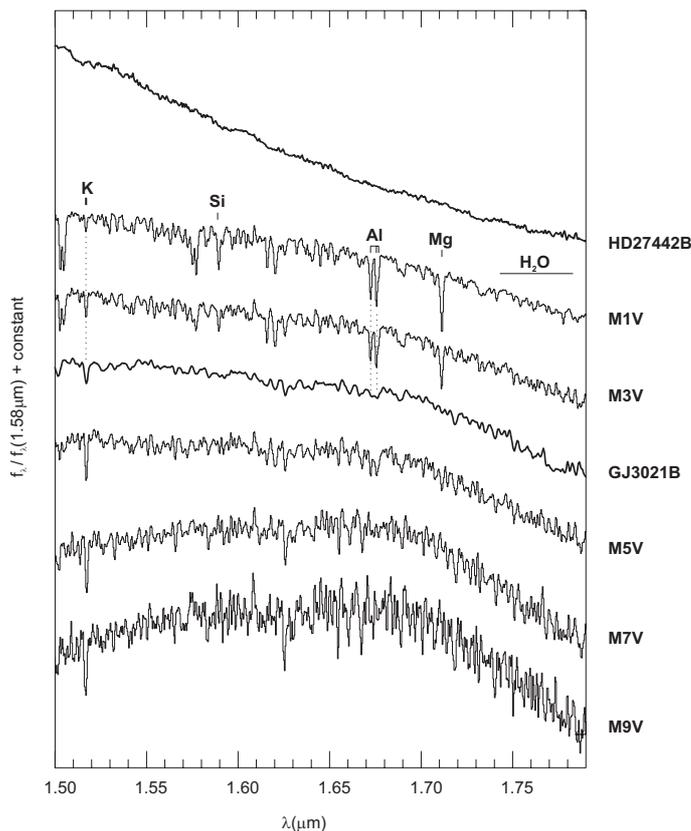
Fig. 12. Our flux-calibrated H-band ISAAC spectra of the co-moving companions GJ 3021 B and HD 27422 B. In addition we show M1V to M9V comparison spectra from Cushing et al. (2005).
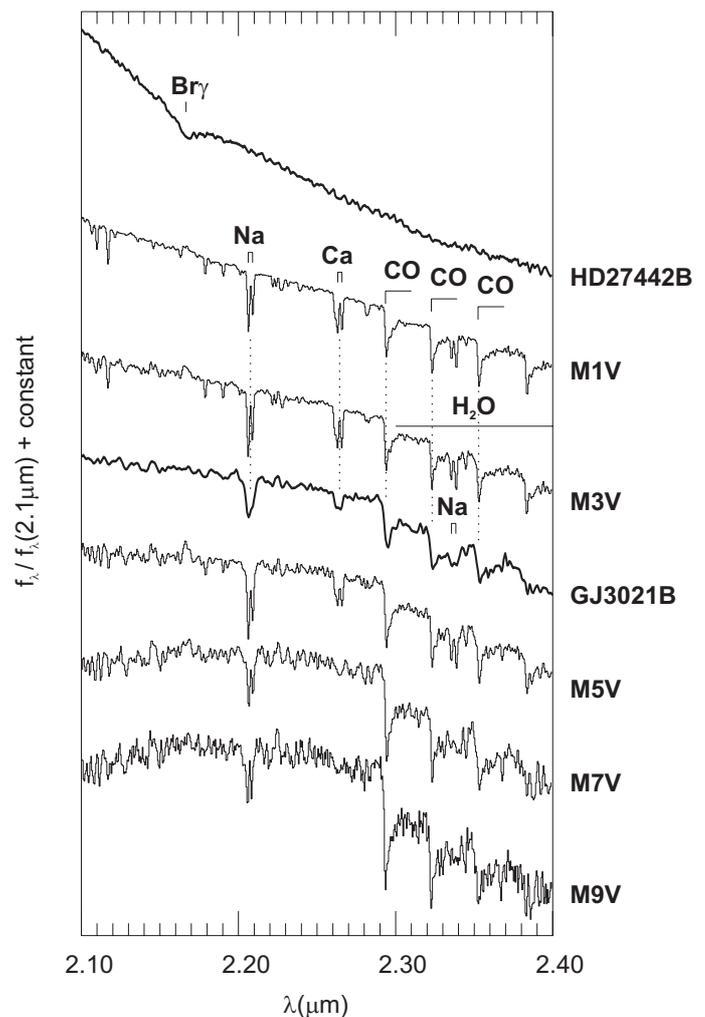

Fig. 13. The flux-calibrated K-band ISAAC spectra of GJ 3021 B and HD 27442 B, together with M1V to M9V comparison spectra from Cushing et al. (2005).

K-band spectra of GJ 3021 B and HD 27442 B are shown in Figs. 12 and 13, together with comparison spectra of dwarfs with spectral types between M1 and M9 from Cushing et al. (2005).

The most dominant absorption feature in the H-band spectrum of GJ 3021 B is the potassium line at 1.52μm. The Mg absorption line at 1.71μm was not detected. Instead, we find the faint absorption features of Al at 1.67μm. The shape of the continuum is consistent with a spectral type between M3 and M5.

In the K-band spectrum of GJ 3021 B, we find atomic absorbtion features of sodium at 2.21μm and 2.33μm, calcium at 2.26μm, and the series of the first-overtone band heads of CO which extend redward of 2.29μm. The strength of the molecular features compared with detected atomic lines is a sensitive indicator of the luminosity class. For equal spectral types the molecular absorption features are more prominent in stars with lower surface gravities (e.g. giants) than in main sequence stars. However, the detected atomic absorbtion features of Na and Ca in the K-band spectrum of GJ 3021 B are comparable to the CO molecular band heads; i.e. GJ 3021 B is a dwarf with a spectral type M3V to M5V.

Our photometric and astrometric results corroborate the results of Chauvin et al. (2006), which show that GJ 3021 B is a co-moving companion with a photometry compatible with what is expected for a mid-M dwarf. Our ISAAC spectroscopy unambiguously confirmed this approximation and finally confined the spectral type of the companion to M4+-1V.

The H- and K-band spectra of HD 27442 B are clearly different from the comparison M-dwarf spectra shown in Figs. 12 and 13. The H- and K-band continua are even steeper than the earliest comparison dwarf M1, indicating a high effective temperature hotter than 3700 K (M1). The H-band spectrum is featureless, whereas we find the Br$_\gamma$ line at 2.16μm in the K-band. This absorption feature is most prominent in B to late F spectral types and it weakens towards spectral types of early K ($T_{\rm eff} > 5000$ K, see Wallace & Hinkle 1997).

Our H- and K-band spectroscopy clearly confirms that HD 27442 B is not a cool low-mass M-dwarf companion. Instead, the lower limit of its effective temperature is consistent with the white dwarf hypothesis, which was concluded in Sect. 2 from photometric data alone. Furthermore, the detected Br$_\gamma$ line indicates that HD 27442 B exhibits a hydrogen atmospheric layer, and we expect to find more typical hydrogen lines in the spectrum of this companion. However, no other lines of the Bracket series are visible in the H-band. To confirm the presence of Hydrogen in the atmosphere of HD 27442 B, we also obtained optical spectra of this companion, reported in the next section.

3.2. Optical spectroscopy of HD 27442 B

We observed HD 27442 B in December 2004 at Paranal Observatory with the second visual and near-UV FOcal Reducer and low dispersion Spectrograph (FORS2), which is installed on the Cassegrain focus of UT1 (Antu). FORS2 is equipped with a mosaic of two MIT CCD detectors, each a 4096×2048 pixel
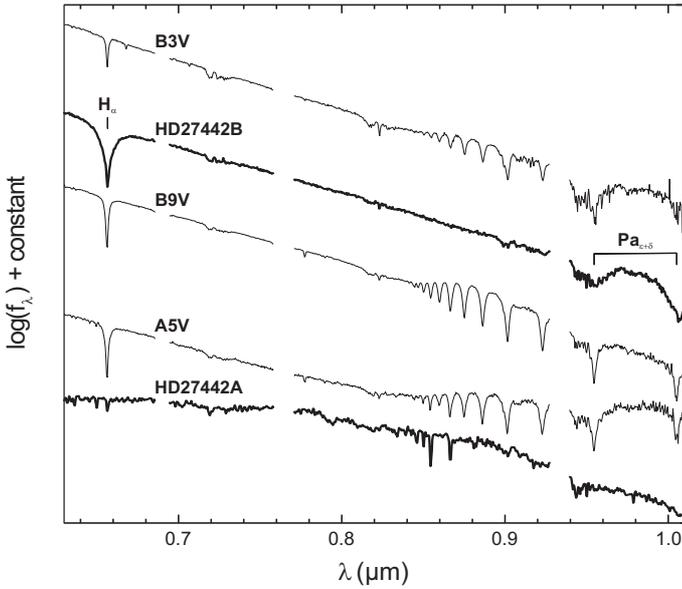
Fig. 14. The FORS2 spectrum of the exoplanet host star HD 27442 A (K2IV) and its co-moving companion HD 27442 B, together with reference spectra with spectral types from mid B to mid A from Danks & Dennefeld (1994). Prominent telluric absorption features are blanked in all spectra.

array with a pixel scale of 0.126 arcsec per pixel. For long-slit spectroscopy, we used the 300I+21 grism combined with the order-sorting filter OG590. With the 1 arcsec slit and the standard resolution collimator, we obtained a resolving power of $\lambda/\Delta\lambda = 660$ at the central wavelength $0.86\,\mu$m. The CCD arrays were operated with a 2×2 pixel binning and a dispersion of $3.22\,$Å per pixel.

We took 8 FORS spectra of HD 27442 B, each with an integration time of 200 s. Between the exposures the telescope was nodded along the slit to avoid always taking the spectrum by the same pixel (bad pixel correction). The bias level was removed, from each spectrum, which was then flat-fielded with a screen flat-field image. Finally all spectra were wavelength-calibrated with a composite spectrum of a helium-argon lamp. The slit was orientated in such a way that the companion and a small part of the primary PSF were always located on the slit. In this way we simultaneously obtained spectra of the companion and of the primary whose spectral type is well-known (K2IV) and can be used for flux calibration. We derived the response function of the spectrograph using the primary spectrum and flux-calibrated reference spectra from Danks & Dennefeld (1994)[7].

We show the flux-calibrated spectra of the exoplanet host star HD 27442 A and its co-moving companion HD 27442 B in Fig. 14, together with comparison spectra of mid B to mid A dwarfs from Danks & Dennefeld (1994). The most striking telluric absorption features are blanked in all spectra. The spectrum of HD 27442 B is clearly different from the primary spectrum, and it exhibits a much steeper continuum. This continuum is comparable to the continua of mid to late B dwarfs with spectral types in the range B3 (11 000 K) and B9 (19 000 K). Furthermore, we detected hydrogen absorption lines, which are all much broader than the absorption lines of the comparison dwarfs. The line broadening is attributed to a high surface gravity and is typical of the absorption lines of white dwarfs. The most prominent hydrogen absorption feature is the Balmer

line H_α at $0.66\,\mu$m. We also find two broadened lines of the Paschen series – Pa_ϵ at $0.95\,\mu$m and Pa_δ at $1.01\,\mu$m.

We detected in total four Hydrogen absorption features in the visible and near infrared spectral range. Our photometric and astrometric results corroborate the results of Chauvin et al. (2006), which show that HD 27442 B is a co-moving companion with a visible and infrared photometry compatible with that expected for a white dwarf. Finally, our ISAAC and FORS2 spectroscopic observations unambiguously confirm the white dwarf nature of HD 27442 B.

The companionship of HD 40979 B+C has so far been proven only with astrometry; i.e. the companions clearly share the proper motion of the exoplanet host star HD 40979 A. With the derived absolute magnitudes of the B and C components, we can derive the expected $V - K$ colors of these two stars using the Baraffe et al. (1998) models. We get $V - H \sim 2.4$ for HD 40979 B and $V - H \sim 4.2$ for HD 40979 C. According to the color-spectral type conversion of Kenyon & Hartmann (1995), these colors correspond to spectral types of K3 and M3, respectively. We also plan to take follow-up spectra to confirm these results.

4. Exoplanet host stars in multiple-star systems

Eggenberger et al. (2004) have already compiled a list of 14 planet host stellar systems, and until end of 2005, two other systems have been reported – HD 142022 (Eggenberger, Mayor, Naef, Pepe, Queloz, Santos, Udry, & Lovis 2005) and HD 188753 (Konacki 2005a).

In addition to our multiplicity study of the exoplanet host stars, we also identified other exoplanet host stars listed as binaries in the WDS catalogue – 83 Leo B, HD 109749, HD 222582, and HD 142. The proper motions of both components of 83 Leo B, HD 109749, and HD 222582 are listed in either the Hipparcos or UCAC2 astrometric catalogues, and the apparent 2MASS photometry of the co-moving companions is consistent with low-mass stars located at the distances of the exoplanet host stars. Thus, the multiplicity of these systems is confirmed by both astrometry and photometry.

The third star, HD 142, is a close binary with separation of ∼5 arcsec) and is listed in the WDS with 5 astrometric measurements. We observed HD 142 with SofI in December 2002 and again in June 2003. According to the Hipparcos astrometry, the expected motion of the primary between the two observations is $PM_{Dec} = 357 \pm 1$ mas and $PM_{Dec} = 5 \pm 1$ mas. With both SofI images, we obtained the proper motion of the WDS companion $PM_{Ra} = 345 \pm 30$ mas and $PM_{Dec} = 43 \pm 30$ mas, which confirms the common proper motion of the pair. The photometry of the B component is contaminated in the 2MASS images by the flux of the nearby bright exoplanet host star; hence, the 2MASS photometry is very uncertain ($H = 5.246$ mag, no magnitude error given here). However, the co-moving companion is well-separated from the primary in our SofI H-band images. We determined its apparent H-band magnitude $H = 7.613 \pm 0.031$ mag. With the Hipparcos parallax of the primary (39.00 ± 0.64 mas), this yields the absolute magnitude of the companion $M_H = 5.568 \pm 0.047$ mag. According to the magnitude-mass relation of the evolutionary Baraffe et al. (1998) models, this magnitude corresponds to a mass of $0.56\,M_\odot$ assuming a system age of 5 Gyr (see Table 6).

The updated list of planet host multiple-star systems is presented in Table 6. We list the mass of the exoplanet host stars and of the secondaries. If the secondary itself is a binary system, we always show the total mass of the pair and add S+S in the case of

---

[7] Telluric absorption features not removed in these spectra.

Table 6. Double and triple stars among the exoplanet host stars.

Planet host star	Mass$_{\rm Host}$ [$M_\odot$]	Mass$_{\rm Comp}$ [$M_\odot$]	$a_{\rm Bin}$ [AU]	$e_{\rm Bin}$	μ	$a_{\rm c}$ [AU]	$a_{\rm P}$ [AU]	P [days]	e	$m\sin(i)$ [$M_{\rm Jup}$]	K [m s^{-1}]	ID	Ref.
Class-1 systems: a,e assumed													
55 Cnc A	0.87	0.27	1062	0.5	0.233	164	0.04	3	0.17	0.05	6.7	e	McArthur (2004)
							0.12	15	0.02	0.78	67.4	b	McArthur (2004)
							0.24	44	0.44	0.22	13.0	c	McArthur (2004)
							5.26	4517	0.33	3.91	49.8	d	McArthur (2004)
83 Leo B	0.78	0.9	502	0.5	0.537	57	0.12	17	0.05	0.11	10.5	b	Marcy (2005)
GJ 3021 A	0.99	0.13	68	0.5	0.112	12	0.49	134	0.51	3.37	167	b	Naef (2001a)
GJ 777 A	0.96	0.2	2841	0.5	0.172	462	0.13	17	0.01	0.06	4.6	c	Vogt (2005)
							3.92	2891	0.36	1.50	23.5	b	Vogt (2005)
Gl 86 A	0.70	0.55	21	0.5	0.440	3	0.11	16	0.05	4	380	b	Queloz (2000)
HD 109749 A	1.04	0.18	489	0.5	0.144	81	0.06	5	0.01	0.28	28.8	b	Fischer (2006)
HD 114729 A	0.97	0.25	282	0.5	0.207	44	2.08	1135	0.32	0.84	18	b	Butler (2003)
HD 114762 A	0.81	0.09	134	0.5	0.097	23	0.34	84	0.35	9	590	b	Mazeh (1996)
HD 142 A	1.28	0.56	104	0.5	0.305	15	1.0	339	0.37	1.03	30	b	Tinney (2002)
HD 142022 A	0.99	0.66	731	0.5	0.401	96	3.03	1928	0.53	5.1	92	b	Eggenberger (2006)
HD 16141 A	1.05	0.29	223	0.5	0.214	35	0.35	76	0.28	0.22	11	b	Marcy (2000)
HD 195019 A	1.06	0.67	128	0.5	0.387	17	0.13	18	0.02	3.47	272	b	Vogt (2000)
HD 196050 A	1.15	0.36	510	0.5	0.240	78	2.4	1300	0.19	2.8	49	b	Jones (2002)
HD 213240 A	1.22	0.15	3899	0.5	0.107	668	2.03	951	0.45	4.5	91	b	Santos (2001)
HD 222582 A	1.02	0.38	4596	0.5	0.272	684	1.35	576	0.71	5.29	184	b	Vogt (2000)
HD 27442 A	0.98	0.58	236	0.5	0.372	32	1.16	415	0.06	1.35	33	b	Butler (2001)
HD 46375 A	0.82	0.58	346	0.5	0.413	45	0.04	3	0.04	0.25	35	b	Marcy (2000)
HD 75289 A	1.23	0.14	621	0.5	0.099	107	0.05	4	0.02	1.15	54	b	Udry (2000)
HD 80606 A	1.04	0.90	1200	0.5	0.466	147	0.47	112	0.93	3.90	411	b	Naef (2001)
HD 89744 A	1.53	0.08	2456	0.5	0.049	440	0.88	256	0.70	7.2	257	b	Korzennik (2000)
υ And A	1.30	0.19	749	0.5	0.125	127	0.06	5	0.04	0.72	74	b	Butler (1999)
							0.83	242	0.23	1.98	56	c	Butler (1999)
							2.50	1269	0.36	4.11	70	d	Butler (1999)
HD 40979 A	1.21	1.21 (S+S)	6416	0.5	0.500	756	0.83	263	0.25	3.28	101	b	Fischer (2003)
HD 41004 A	0.91	0.59 (S+B)	23	0.5	0.395	3	1.7	963	0.74	2.54	99	b	Zucker (2004)
HD 178911 B	0.98	1.88 (S+S)	784	0.5	0.657	76	0.32	72	0.12	6.29	339	b	Zucker (2002a)

Planet host star	Mass$_{\rm Host}$ [$M_\odot$]	Mass$_{\rm Comp}$ [$M_\odot$]	$a_{\rm Bin}$ [AU]	$e_{\rm Bin}$	μ	$a_{\rm c}$ [AU]	$a_{\rm P}$ [AU]	P [days]	e	$m\sin(i)$ [$M_{\rm Jup}$]	K [m s^{-1}]	ID	Ref.
Class-2 systems: a,e known													
γ Cep A	1.59	0.41	19	0.361	0.207	4	2.13	906	0.12	1.7	28	b	Hatzes (2003)
HD 19994 A	1.37	0.62	151	0.26	0.310	36	1.42	536	0.30	1.68	36	b	Mayor (2004)
τ Boo A	1.33	0.44	98	0.4189	0.247	18	0.05	3	0.02	3.87	469	b	Butler (1997)
HD 188753 A	1.06	1.63 (S+S)	12	0.5	0.606	1	0.05	3	0	1.14	149	b	Konacki (2005)
16 Cyg B	0.99	1.18 (S+S)	755	0.863	0.543	15	1.6	801	0.63	1.5	44	b	Cochran (1997)

Remarks:

55 Cnc A:	separation and mass of B component from Mugrauer et al. (2006), this also holds for HD 80606 A and HD 46375 A.
83 Leo B:	fainter B component is the exoplanet host star whose mass is estimated by Marcy et al. (2005).
Gl 86 A:	B is a white dwarf; separation and mass estimated by Mugrauer & Neuhäuser (2005).
HD 142 A:	mass of B component determined with our SofI H-band photometry.
HD 109749 A:	mass of primary from Allende Prieto & Lambert (1999).
HD 114729 A:	separation and mass of B component from Mugrauer et al. (2005), this also holds for HD 196050, HD 213240 and HD 16141.
HD 114762 A:	mass of B component determined with 2MASS K-band photometry (A+B unresolved) and $\Delta{\rm K}_{AB}$ from Patience et al. (2002).
HD 142022 A	mass of primary from Eggenberger et al. (2005).
HD 27442 A:	primary mass from Randich et al. (1999).
HD 75289 A:	separation and mass of companion from Mugrauer et al. (2004a).
HD 89744 A:	separation and mass of companion from Mugrauer et al. (2004b).
HD 40979 A:	triple system A/B+C; mass of B and C component are derived with I-band MONICA photometry (see Sect. 2).
HD 41004 A:	triple system A/B+C with a brown-dwarf companion (C); the separation between A and B+C is measured by Hipparcos; primary mass from Allende Prieto & Lambert (1999) and mass of B component is derived with Hipparcos photometry; mass of brown-dwarf companion estimated with radial velocity data from Zucker et al. (2004).
HD 19994 A:	mass of B component derived with 2MASS K-band photometry (A+B unresolved) and $\Delta K_{AB} = 3.0 \pm 0.1$ mag measured by us with NACO/VLT in run 073.C-0370(A).
τ Boo A:	mass of B component determined with 2MASS K-band photometry (A+B unresolved) and ΔK_{AB} from Patience et al. (2002).
HD 188753 A:	triple system A/B+C, all masses from Konacki (2005a).
HD 178911 B:	triple system A+C/B, masses of A and C component from Tokovinin et al. (2000).
16 Cyg B	triple system A+C/B, mass of C component is determined with 2MASS H-band photometry (A+C unresolved) and $\Delta{\rm H}_{AC}$ from Patience et al. (2002).
γ Cep:	orbital solution and mass determination of B component with radial velocity data from Hatzes et al. (2003); mass of A component from Fuhrmann (2004).

two stars or S+B in the case of a star with a brown-dwarf companion. We derive the ratio between the companion mass and the total system-mass (μ), as well as the critical semi-major axes (a_c). We also list the orbital properties of all exoplanets detected in these stellar systems.

We consider here only systems whose exoplanets ($m \sin(i) <$ 13 M_{Jup}) are published in refereed papers until the end of 2005. We excluded two systems from the table – the WDS binary HD 11964, and the triple system HD 219449 A+BC, because the exoplanets in these stellar systems were both announced, but not published in a refereed paper. In total, the table includes 29 systems, 24 binaries, and 5 triple systems – HD 188753, 16 Cyg, HD 178911, HD 40979, and HD 41004.

The whole sample can be subdivided into two classes of systems. Class-1 systems are confirmed common-proper-motion pairs whose projected separations are known from astrometric measures but their orbital parameters (e.g. semi-major axes, eccentricity) are unknown. For these systems we always used the projected separations as an estimate of the semi-major axes and assumed an orbital eccentricity of $e = 0.5$, which is a good estimate for wide multiple-star systems (see e.g. eccentricity distribution of wide binaries from Söderhjelm 1999). For 5 systems, only the orbital parameters are known from either astrometric (Hartkopf et al. 2005) or radial-velocity measurements (Hatzes et al. 2003). These special systems are denoted as Class-2 systems.

In the majority of cases (exceptions are summarized under remarks in Table 6), we derived the masses of the companions using their apparent 2MASS infrared magnitudes, the Hipparcos parallaxes of the exoplanet host stars, and the magnitude-mass conversion of the 5 Gyr Baraffe et al. (1998) models. For the masses of the exoplanet host stars, we used the mass-estimates from Santos et al. (2004), if available (for exceptions see remarks in Table 6).

With the masses and semi-major axes from Table 6, we can derive the orbital periods of all planet host stellar systems and compare their distribution with the period distribution of an unbiased comparison binary sample with G type primaries (Duquennoy & Mayor 1991), which are both shown in Fig. 15. We determined the semi-major axes of Class-1 systems with the relation between semi-major axes a and projected separations sep also used by Duquennoy & Mayor (1991) ($\log(a/\mathrm{sep}) =$ 0.13). For Class-2 systems, we used the given orbital periods derived from orbit fitting. Apparently, there is a lack of close planet host stellar systems. Most of the detected planet host binaries are found with orbital periods $6 < \log(P[\mathrm{days}]) < 7$ while the unbiased control sample exhibits its peak in the period bin $4 < \log(P[\mathrm{days}]) < 5$.

The difference between the two period distributions is probably the result of an observational selection effect, due to the difficulty detecting planets in close binary systems using the radial-velocity technique. If we assume a limit-angular separation of 2.5 arcsec for the planet search in binaries, this yields a limiting orbital period of $\log(P[\mathrm{days}] \sim 5.6$, calculated with the average distance of the exoplanet host stars (40 pc) and a binary total mass of 1 $M_\odot$. Indeed, we count only 6 planet host binaries with shorter orbital periods and 23 with longer orbital periods. Most of these close systems are composed of a bright exoplanet host star and a much fainter secondary star that does not disturb the radial-velocity planet search technique. Only a systematic planet-search in wide and close binary systems would be able to indicate whether planet host binaries tend to be more widely separated than binaries without planets.
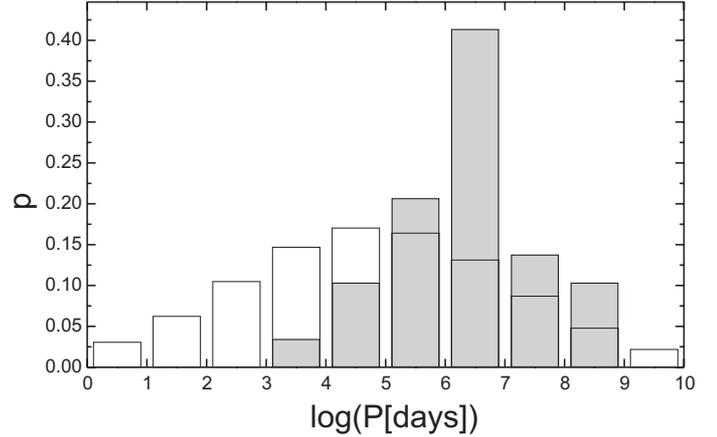
Fig. 15. The relative frequencies of the approximated orbital periods of planet host binaries (grey bars) and an unbiased comparison binary sample (Duquennoy & Mayor 1991) with G type primaries (white bars).
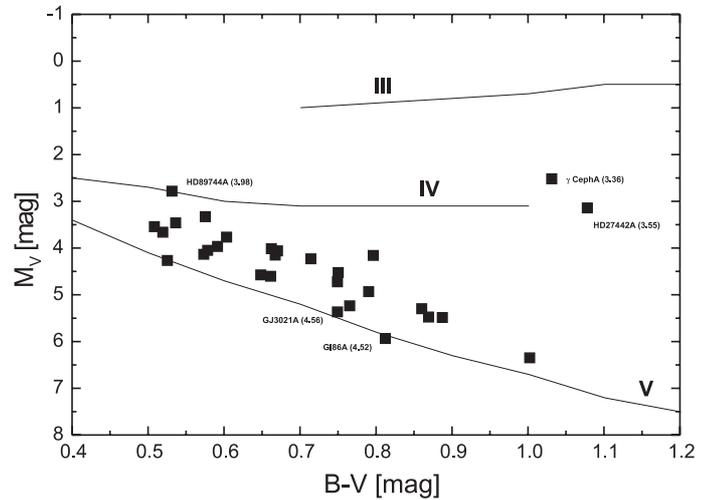
Fig. 16. Hipparcos photometry of all exoplanet host stars located in multiple-star systems. The absolute V-band magnitudes are obtained with distances derived from the Hipparcos parallaxes. For comparison we show the expected colors and magnitudes of dwarfs, subgiants, and giants taken from Schmidt-Kaler (1982).

Most of the exoplanet host stars that reside in multiple-star systems are dwarfs with spectral types between late F and early K. Their properties are well-known, derived from spectroscopy and astrometry. The location of these stars in a color-magnitude diagram is shown in Fig. 16. The absolute V-band magnitudes are determined with distances from Hipparcos (Perryman & ESA 1997), which also provides the V- and B-band photometry. For comparison, we plot continuous lines that present the intrinsic colors and magnitudes of dwarfs, subgiants, and giants (data from Schmidt-Kaler 1982). The brightest and most evolved stars in the sample are HD 89744 A, γ Cep A, and HD 27442 A.

HD 89744 A is classified as an F7V dwarf. However, both its low surface-gravity $\log(g[\mathrm{cm/s^2}]) = 3.98 \pm 0.05$ (Santos et al. 2004) and its position in the color-magnitude diagram are only marginally consistent with the dwarf classification, which indicates that this star has already evolved.

The planet host star γ Cep A (Hatzes et al. 2003) is listed in the Hipparcos catalogue as a subgiant with a spectral type K1IV.

Santos et al. (2004) derive a surface gravity of $\log(g[\text{cm/s}^2]) = 3.36 \pm 0.21$, which is consistent with the subgiant classification. The star γ Cep is a single-lined spectroscopic binary system (Campbell, Walker, & Yang 1988), whose secondary, γ Cep B, was also recently detected directly by Neuhäuser et al. (2007).

As described in Sect. 2.2, HD 27442 A is an evolved early K type subgiant. The derived spectral type and its luminosity class are both fully consistent with its position in the color-magnitude diagram in Fig. 16. Furthermore, this binary system is a special case among all known planet host binary systems. With its subgiant exoplanet host star and the white dwarf companion HD 27442 B, it is the most evolved planet host stellar system known today.

5. Discussion

5.1. Long-term stability of exoplanets in multiple-star systems

According to Holman & Wiegert (1999) planets in binary systems are stable on a long timescale only if their semi-major axes (circular orbit assumed) do not extend a critical value, the so-called critical semi-major axis a_c. This axis depends on the mass-ratio of the primary and secondary ($\mu = m_{Sec}/(m_{Prim} + m_{Sec})$), as well as on the binary eccentricity. We followed Holman & Wiegert (1999) prescription and derived in Table 6 the critical semi-major axis for all the multiple-star systems with exoplanets.

The derived critical semi-major axes range from 1 AU (HD 188753) up to 800 AU (HD 40979). They can be used to estimate the long-term stable regions of additional planets or brown-dwarf companions in these systems around the planet host stars. Only four planet host multiples are presently known to have critical semi-major axes below 5 AU. These are HD 188753 (1 AU), HD 41004 (3 AU), Gl 86 (3 AU), and γ Cep (4 AU). Note that all four exoplanets reside within the proposed long-term stable regions. However, the existence of gaseous giant, Jovian-like planets on orbits similar to planets in our own solar system ($a > 5$ AU) are not stable in these systems. Furthermore, Uranus-or Neptune-like orbits, with a separation between 20 and 30 AU, as well as Kuiper belts that extend beyond 20 AU, can be ruled out in about a third of all planet host stellar systems.

The extent of the long-term stable regions changes during the post-main sequence evolution of the stellar system. Due to the mass-loss of the stars, the binary mass-ratio μ and its semi-major axis change lead to a variation of the long-term stable regions around the individual stars. An interesting example of this effect is the binary system HD 27442 AB, a wider analog to the Gl 86 AB system (see Mugrauer et al. 2005a; Lagrange et al. 2006). With a white dwarf companion and a subgiant planet host star, it is the most evolved planet host binary system known today. According to the initial to final mass-relation from Weidemann (2000), the white-dwarf progenitor was most probably a solar-like star. Due to the mass-loss during the red-giant phase of the white-dwarf progenitor, the binary semi-major axis had to expand slightly by a factor of ~1.7, i.e. from ~140 AU to the current value of ~240 AU. Due to these variations the long-term stable region around the exoplanet host star extended from 14 AU up to 32 AU. The known exoplanet that revolves around HD 27442 A in its 1.2 AU circular orbit was well within the smaller long-term stable region and was therefore not dynamically affected, even before the mass-loss of the secondary star.

The known exoplanet survived the mass-loss of HD 27442 B but might not survive the evolution of its parent star. HD 27442 A is already slightly evolved and will pass through the final stages of stellar evolution in the next few hundred million years. Livio & Soker (1984) showed that, during the red-giant phase of its parent star, a close enough planet spirals inwards, which results in evaporation of the planet atmosphere that eventually dissolves the planet in only a few thousand years. Therefore, the presently known planet probably will not last for more than a few million years. Other planets in the system with separations larger than ~5 AU might survive the red-giant stage (Burleigh et al. 2002) while their orbits expand by a factor of two. Their orbit will still remain within the long-term stable region around HD 27442 A. Also, HD 27442 B might have wide survivor planets, orbiting the white dwarf in its long-term stable of about 20 AU (1 arcsec).

5.2. Statistical differences between single-star and multiple-star planets

Differences in the mass-period and eccentricity-period correlation between the single- and multiple-star planets have been already pointed out by Zucker & Mazeh (2002) and Eggenberger et al. (2004). These authors note that in the mass-period diagram for orbital periods shorter than 40 days, massive planets ($m \sin(i) > 2\,M_{Jup}$) are only found among the multiple-star planets, whereas all the detected single-star planets have lower masses. In contrast, multiple-star planets exhibit only masses lower than $5\,M_{Jup}$ for orbital periods longer than 100 days, whereas the masses of single-star planets clearly extend beyond this mass-limit. The two populations seem different in the eccentricity-period diagram as well. For orbital periods shorter than 40 days multiple-star planets revolve around their parent stars only on almost circular orbits ($e \leq 0.05$), whereas single-star planets could have higher orbital eccentricities, up to ~0.5. We can check these conjectures now with the updated enlarged dataset.

As listed in Table 6, 35 of the exoplanets are known to orbit a star that is a member of binary or even triple-star systems. Among those stellar systems, we also find apparently wide systems with approximated semi-major axes of more than 2000 AU (GJ 777, HD 2132140, HD 222582, HD 89744, and HD 40979). From the theoretical point of view, it might be difficult to imagine the influence of those wide companions on the formation and orbital evolution of exoplanets, even with the Kozai effect and migration scenario. However, as already described in the previous section, the orbital elements are only approximated (Class-1 systems) for the majority of these stellar systems. Therefore, it might be possible that these apparently wide systems exhibit much smaller semi-major axes with high orbital eccentricities. Furthermore, presently wide binary systems might have been much closer in the past, because the orbital elements of the binary systems could also have been altered, e.g., due to close encounters with other stars during the system formation either in a stellar cluster or later in the galactic plane. Note also that evolved systems with white-dwarf companions have expanded their semi-major axes due to mass-loss of the white-dwarf progenitors. We therefore decided to analyze all multiple-star planets as one group and compare them with the single-star planets.

To avoid selection effects we discarded all planets with small radial-velocity amplitudes $K < 15$ m/s. In particular 5 multiple-star planets, namely 55 Cnc e and c, 83 Leo b, GJ 777 c, and HD 16141 b, are not considered in the analysis because of their low radial-velocity amplitudes. Altogether we had 108 single-star and 30 multiple-star planets by the end of 2005.

The correlation diagrams of both planet populations are shown in Fig. 17, together with the mass- and eccentricity-limits for short and long-period planets as proposed by Eggenberger et al. (2004) (see dotted lines in Fig. 17). In the updated planet sample, the mass-limit has to be increased from 2 to 2.5 M_{Jup} due to the single-star planet HD 188203 b, which slightly extends the mass-limit proposed by Eggenberger et al. (2004).

In the short-period domain, $P < 40$ days, we count 30 single-star and 6 multiple-star planets with $m \sin(i) \le 2.5 M_{Jup}$. There are 3 multiple-star planets with $m \sin(i) > 2.5 M_{Jup}$ and no single-star planet. If we assume that both planet populations have the same mass-period distribution, the probability of the given planet distribution can be derived with a hypergeometric distribution, which yields a probability of 0.92%[8].

Eggenberger et al. (2004) also suggest that the planets in multiple-star systems with orbital periods longer than 100 days are less massive. However, in the updated plot, three multiple-star planets (HD 89744 b, HD 222582 b, HD 142022 b) exceed the proposed mass-limit ($m \sin(i) < 5 M_{Jup}$) for the given range of orbital periods. These outliers substantially weaken the significance of the suggested feature.

In the updated eccentricity-period diagram, we count 18 single-star planets and 9 multiple-star planets all on almost circular orbits ($e \le 0.05$), and 12 single-star planets with $e > 0.05$ all with periods shorter than 40 days. There is no multiple-star planet found on an eccentric orbit for the given range of orbital periods. If we assume that there is no difference in the eccentricity-period distribution of both exoplanet populations, the probability for the given planet distribution is 2.21%[9]. This result is similar to the 3.77%, reported by Eggenberger et al. (2004). The remaining correlation of the planet properties, namely the eccentricity-mass correlation is shown in the bottom panel of Fig. 17. The mass-eccentricity distributions of both planet populations seem similar, with no significant statistical difference.

In addition to the analysis of the correlation diagrams, we also compared the period, eccentricity, and mass-distribution functions of both planet populations. The three cumulative distribution functions F are plotted in Fig. 18. The cumulative functions of the orbital parameters (period $F(P)$ and eccentricity $F(e)$) of both planet populations appear to be more or less identical with only small variations. In contrast, the mass-distributions $F(m \sin(i))$ seem different, although Kolmogorov-Smirnov (K-S) two-sample test indicates that the hypothesis that the two distributions are equal can be rejected with only 81% significance level. The biggest discrepancy (D_{max}) between both cumulative mass-functions appears at about 3 M_{Jup} (see Fig. 18).

In a further step in examining the possible difference between the mass-distributions, we derived the underlying density functions from the cumulative distribution functions. To derive these function we interpolated the cumulative mass-distribution functions of both planet populations using 1000 data points spanning a range of mass from 0 to 13 M_{Jup}. We apply an adjacent averaging with a boxwidth of 50 data points. The value y_i for each point x_i is the average of the values of all points in the interval $[x_{i-25}; x_{i+25}]$.

The derivative is taken by averaging the two adjacent data slopes at point x_i: $f'(x_i) = \frac{1}{2}\left(\frac{y_{i+1}-y_i}{x_{i+1}-x_i} + \frac{y_i-y_{i-1}}{x_i-x_{i-1}}\right)$. High spatial

---

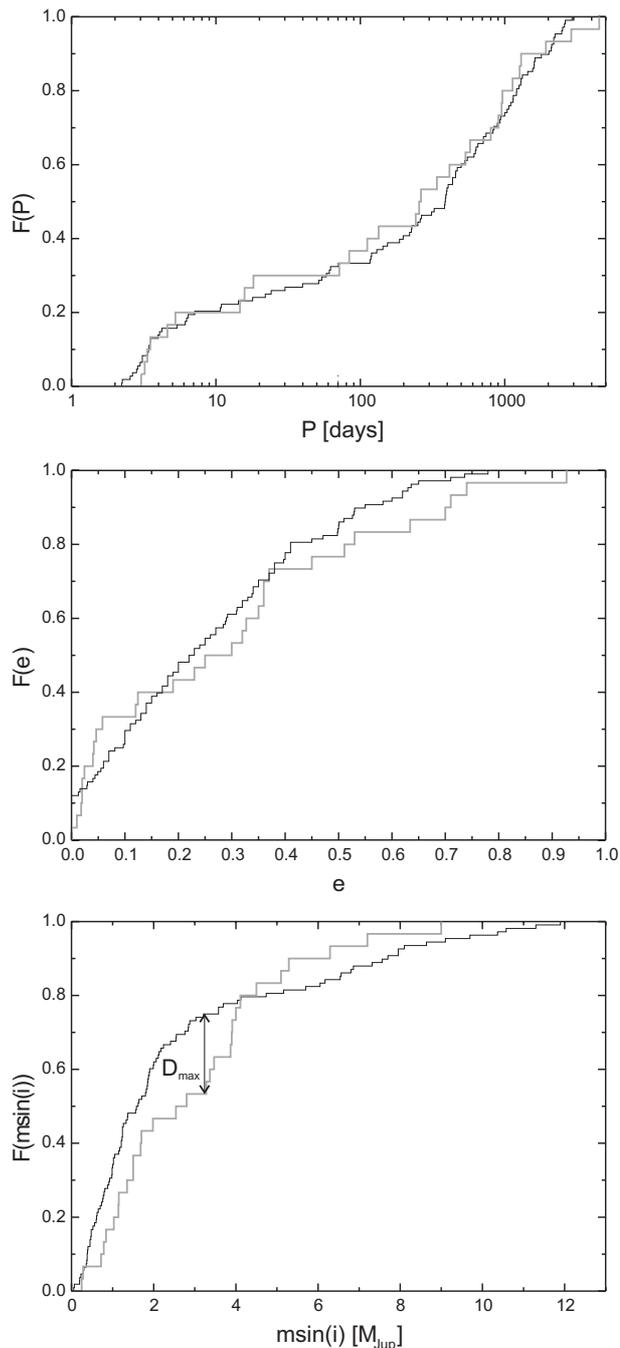[8] Hypergeometric distribution: $\binom{36}{6}\binom{3}{3} / \binom{39}{9} = 0.92\%$.

[9] Hypergeometric distribution: $\binom{27}{9}\binom{12}{0} / \binom{39}{9} = 2.21\%$.
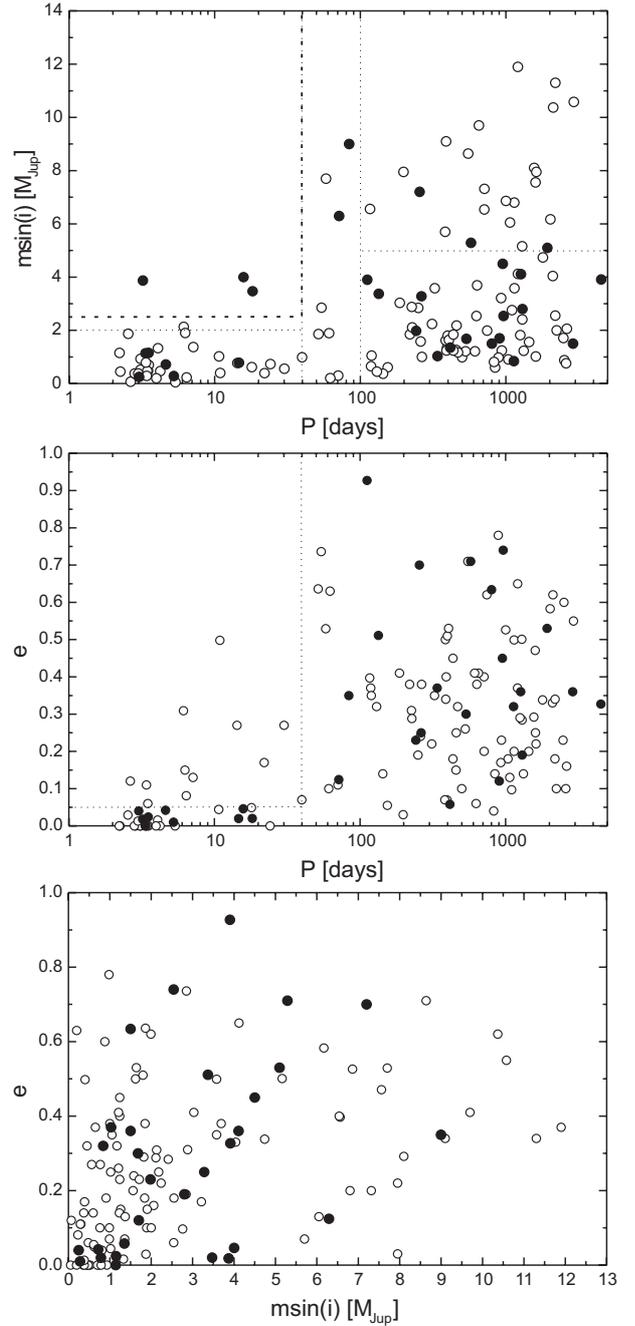
Fig. 17. The mass-period (*top*), eccentricity-period (*middle*), and eccentricity-mass (*bottom*) correlation diagrams of single-star (open circles) and multiple-star planets (filled circles). The mass and eccentricity-limits, as proposed by Eggenberger et al. (2004), are illustrated with dotted lines. The updated mass-limit for short period planets is shown as a thick dashed line. Only planets with $m \sin(i) < 13 M_{Jup}$ and $K > 15$ m s^{-1} are taken into account.
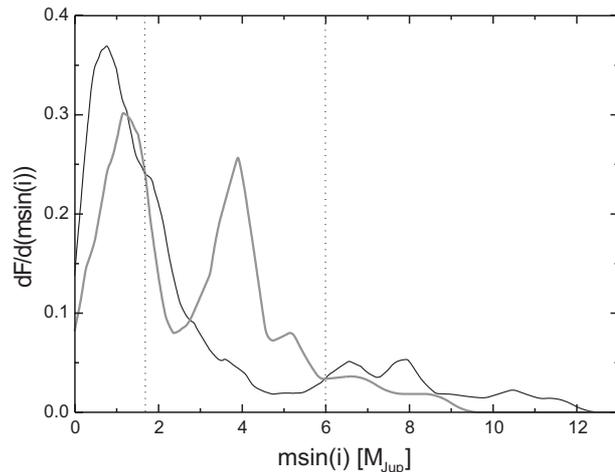
frequencies are smoothed again with an adjacent average with a boxwidth of 50 data points. The derived mass-distribution functions are shown in Fig. 19.

Both planet populations exhibit a similar mass-distribution in the low-mass and high-mass range, with a high peak at about 1 M_{Jup}, but they differ at the intermediate mass-range, between ∼2 and 6 M_{Jup}. At this range, the multiple-star planets seem to be more frequent than single-star planets. If this difference is true, it might indicate that the planet formation process is indeed altered by the stellar multiplicity. One possibility is that

Fig. 19. The derived mass-distribution of single-star planets (thin black line) and multiple-star planets (thick grey line). The mass-distribution functions are derived from the cumulative mass-distribution functions (see text for more details). More massive single-star planets are less probable, whereas multiple-star planets exhibit another peak in their mass-distribution at about 4 M_{Jup}.

Finally, it is important to mention that all the reported possible differences between the properties of single- and multiple-star planets have to be reexamined when the sample size of planet host stellar systems is significantly extended, at least by a factor of two, i.e. when about 60 such systems are known. While writing the manuscript of this paper, new companions or interesting companion candidates already had been presented (see e.g. Chauvin et al. 2006; Raghavan et al. 2006 and Bakos et al. 2006). In fact, we also plan to show new promising results of our multiplicity study in a forthcoming publication.

6. Summary

1. GJ 3021 B is a close M4V-M5V stellar companion, as confirmed by ISAAC spectroscopy.
2. The wide companion of the binary system HD 40979 AB is resolved in a pair B+C; i.e. this is a new triple-star system that host a planet.
3. HD 27442 B is a co-moving companion of an exoplanet host star whose white dwarf nature, is confirmed by ISAAC and FORS spectroscopy.
4. HD 27442 AB is the most evolved planet host stellar system known today.
5. Massive ($m \sin(i) > 2.5\,M_{\mathrm{Jup}}$) shortperiod planets ($P < 40$ days) apparently all reside in multiple-star systems, probably on almost circular orbits ($e \leq 0.05$).
6. Intermediate-mass planets ($\sim 4 \pm 2\,M_{\mathrm{Jup}}$) might be more frequent in multiple-star systems than around single stars.

Fig. 18. The cumulative functions of planet periods (*top*), eccentricities (*middle*), and masses (*bottom*). The functions of single-star planets are shown as thin black lines and those of multiple-star planets as thick grey lines. All functions are scaled equally on the probability axis; i.e. the three functions can be directly compared with each other. The largest detected difference $D_{\max}$ between both planet populations occurs in the cumulative mass-functions and is indicated by a black line with arrows. Only planets with $m \sin i(i) < 13\,M_{\mathrm{Jup}}$ and $K > 15\,\mathrm{m\,s^{-1}}$ are taken into account.

the mass-accretion rate onto the forming planet embedded in a protoplanetary disk is enhanced (as described by Kley 2000). Another possibility is that, because of the angular momentum transfer from the planet bearing disks to the perturbing companion star, more material resides closer in, which finally allows the formation of more massive planets.

References

Allende Prieto, C., & Lambert, D. L. 1999, A&A, 352, 555
Bakos, G. Á., Pál, A., Latham, D. W., Noyes, R. W., & Stefanik, R. P. 2006, ApJ, 641, L57
Baraffe, I., Chabrier, G., Allard, F., & Hauschildt, P. H. 1998, A&A, 337, 403
Baraffe, I., Chabrier, G., Barman, T. S., Allard, F., & Hauschildt, P. H. 2003, A&A, 402, 701
Bergeron, P., Leggett, S. K., & Ruiz, M. T. 2001, ApJS, 133, 413
Burleigh, M. R., Clarke, F. J., & Hodgkin, S. T. 2002, MNRAS, 331, L41
Butler, R. P., Marcy, G. W., Fischer, D. A., et al. 1999, ApJ, 526, 916
Butler, R. P., Marcy, G. W., Vogt, S. S., et al. 2003, ApJ, 582, 455
Butler, R. P., Marcy, G. W., Williams, E., Hauser, H., & Shirts, P. 1997, ApJ, 474, L115
Butler, R. P., Tinney, C. G., Marcy, G. W., et al. 2001, ApJ, 555, 410
Campbell, B., Walker, G. A. H., & Yang, S. 1988, ApJ, 331, 902
Chauvin, G., Lagrange, A.-M., Udry, S., et al. 2006, A&A, 456, 1165
Cochran, W. D., Hatzes, A. P., Butler, R. P., & Marcy, G. W. 1997, ApJ, 483, 457
Cushing, M. C., Rayner, J. T., & Vacca, W. D. 2005, ApJ, 623, 1115
Cutri, R. M., Skrutskie, M. F., van Dyk, S., et al. 2003, VizieR Online Data Catalog, 2246, 0
Danks, A. C., & Dennefeld, M. 1994, PASP, 106, 382
Desidera, S., Gratton, R. G., Claudi, R. U., et al. 2004, in Extrasolar Planets: Today and Tomorrow, ed. J. Beaulieu, A. Lecavelier Des Etangs, & C. Terquem, ASP Conf. Ser., 321, 103
Devillard, N. 2001, in Astronomical Data Analysis Software and Systems X, ed. F. R. Harnden, F. A. Primini, & H. E. Payne, ASP Conf. Ser., 238, 525
Duquennoy, A., & Mayor, M. 1991, A&A, 248, 485
Eggenberger, A., Mayor, M., Naef, D., et al. 2005, The CORALIE survey for southern extrasolar planets XIV. HD 142022 b: a long-period planetary companion in a wide binary
Eggenberger, A., Udry, S., & Mayor, M. 2004, A&A, 417, 353
Els, S. G., Sterzik, M. F., Marchis, F., et al. 2001, A&A, 370, L1
Fischer, D. A., Marcy, G. W., Butler, R. P., et al. 2003, ApJ, 586, 1394
Fischer, D. A., Laughlin, G., Marcy, G. W., et al. 2006, ApJ, 637, 1094
Ford, E. B., Kozinsky, B., & Rasio, F. A. 2000, ApJ, 535, 385
Fuhrmann, K. 2004, Astron. Nachr., 325, 3
Halbwachs, J. L. 1986, A&AS, 66, 131
Hartkopf, W. I., Mason, B. M., & Worley, C. E. 2005, Sixth Catalog of Orbits of Visual Binary Stars, http://ad.usno.navy.mil/wds/orb6/orb6.html
Hatzes, A. P., Cochran, W. D., Endl, M., et al. 2003, ApJ, 599, 1383
Holman, M. J., & Wiegert, P. A. 1999, AJ, 117, 621
Jahreiß, H. 2001, in Astronomische Gesellschaft Meeting Abstracts, ed. E. R. Schielicke, 110
Jones, H. R. A., Paul Butler, R., Marcy, G. W., et al. 2002, MNRAS, 337, 1170
Kenyon, S. J., & Hartmann, L. 1995, ApJS, 101, 117
Kley, W. 2000, in IAU Symp., 211P
Konacki, M. 2005a, Nature, 436, 230
Konacki, M. 2005b, ApJ, 626, 431
Korzennik, S. G., Brown, T. M., Fischer, D. A., Nisenson, P., & Noyes, R. W. 2000, ApJ, 533, L147
Lagrange, A.-M., Beust, H., Udry, S., Chauvin, G., & Mayor, M. 2006, A&A, 459, 955
Liebert, J., Bergeron, P., & Holberg, J. B. 2005, ApJS, 156, 47
Livio, M., & Soker, N. 1984, MNRAS, 208, 763
Lowrance, P. J., Kirkpatrick, J. D., & Beichman, C. A. 2002, ApJ, 572, L79

Marcy, G. W., Butler, R. P., & Vogt, S. S. 2000, ApJ, 536, L43
Marcy, G. W., Butler, R. P., Vogt, S. S., et al. 2005, ApJ, 619, 570
Marzari, F., & Scholl, H. 2000, ApJ, 543, 328
Mayer, L., Wadsley, J., Quinn, T., & Stadel, J. 2005, MNRAS, 363, 641
Mayor, M., & Queloz, D. 1995, Nature, 378, 355
Mayor, M., Udry, S., Naef, D., et al. 2004, A&A, 415, 391
Mazeh, T., Latham, D. W., & Stefanik, R. P. 1996, ApJ, 466, 415
McArthur, B. E., Endl, M., Cochran, W. D., et al. 2004, ApJ, 614, L81
Mugrauer, M., & Neuhäuser, R. 2005, MNRAS, 361, L15
Mugrauer, M., Neuhäuser, R., Mazeh, T., Alves, J., & Guenther, E. 2004a, A&A, 425, 249
Mugrauer, M., Neuhäuser, R., Mazeh, T., Guenther, E., & Fernández, M. 2004b, Astron. Nachr., 325, 718
Mugrauer, M., Neuhäuser, R., Seifahrt, A., Mazeh, T., & Guenther, E. 2005, A&A, 440, 1051
Mugrauer, M., Neuhäuser, R., Mazeh, T., et al. 2006, Astron. Nachr., 327, 321
Naef, D., Latham, D. W., Mayor, M., et al. 2001a, A&A, 375, L27
Naef, D., Mayor, M., Pepe, F., et al. 2001b, A&A, 375, 205
Neuhäuser, R., Mugrauer, M., Fukagawa, M., Torres, G., & Schmidt, T. 2007, A&A, 462, 777
Patience, J., White, R. J., Ghez, A. M., et al. 2002, ApJ, 581, 654
Perryman, M. A. C., & ESA. 1997, The HIPPARCOS and TYCHO catalogues. Astrometric and photometric star catalogues derived from the ESA HIPPARCOS Space Astrometry Mission (Noordwijk, Netherlands: ESA Publications Division), ESA SP Ser. 1200
Pichardo, B., Sparke, L. S., & Aguilar, L. A. 2005, MNRAS, 359, 521
Pickles, A. J. 1998, PASP, 110, 863
Queloz, D., Mayor, M., Weber, L., et al. 2000, A&A, 354, 99
Raghavan, D., Henry, T. J., Mason, B. D., et al. 2006, ApJ, 646, 523
Randich, S., Gratton, R., Pallavicini, R., Pasquini, L., & Carretta, E. 1999, A&A, 348, 487
Rocha-Pinto, H. J., & Maciel, W. J. 1998, MNRAS, 298, 332
Saffe, C., Gómez, M., & Chavero, C. 2005, A&A, 443, 609
Santos, N. C., Israelian, G., & Mayor, M. 2004, A&A, 415, 1153
Santos, N. C., Mayor, M., Naef, D., et al. 2001, A&A, 379, 999
Schmidt-Kaler, T. 1982, in Landolt-Börnstein, ed. K. Schaifers, & H. Voigt, Vol. 2 (Berlin: Springer), 449
Söderhjelm, S. 1999, A&A, 341, 121
Tinney, C. G., Butler, R. P., Marcy, G. W., et al. 2002, ApJ, 571, 528
Tokovinin, A. A., Griffin, R. F., Balega, Y. Y., Pluzhnik, E. A., & Udry, S. 2000, Astron. Lett., 26, 116
Toyota, E., Itoh, Y., Matsuyama, H., et al. 2005, in Protostars and Planets V, 8247
Udry, S., Mayor, M., Naef, D., et al. 2000, A&A, 356, 590
Vogt, S. S., Butler, R. P., Marcy, G. W., et al. 2005, ApJ, 632, 638
Vogt, S. S., Marcy, G. W., Butler, R. P., & Apps, K. 2000, ApJ, 536, 902
Wallace, L., & Hinkle, K. 1997, ApJS, 111, 445
Weidemann, V. 2000, A&A, 363, 647
Worley, C. E., & Douglass, G. G. 1997, A&AS, 125, 523
Wu, Y., & Murray, N. 2003, ApJ, 589, 605
Zacharias, N., Urban, S. E., Zacharias, M. I., et al. 2004, AJ, 127, 3043
Zucker, S., & Mazeh, T. 2002, ApJ, 568, L113
Zucker, S., Naef, D., Latham, D. W., et al. 2002, ApJ, 568, 363
Zucker, S., Mazeh, T., Santos, N. C., Udry, S., & Mayor, M. 2003, A&A, 404, 775
Zucker, S., Mazeh, T., Santos, N. C., Udry, S., & Mayor, M. 2004, A&A, 426, 695